

Electronic Thesis and Dissertation Repository

---

4-20-2012 12:00 AM

## Enhancing Raman and Fluorescence Spectroscopies with Nanosphere Lithography Platforms

Shabila Fayyaz

*The University of Western Ontario*

Supervisor

Dr. François Lagurné-Labarthe

*The University of Western Ontario*

Graduate Program in Chemistry

A thesis submitted in partial fulfillment of the requirements for the degree in Master of Science

© Shabila Fayyaz 2012

Follow this and additional works at: <https://ir.lib.uwo.ca/etd>

 Part of the [Physical Chemistry Commons](#)

---

### Recommended Citation

Fayyaz, Shabila, "Enhancing Raman and Fluorescence Spectroscopies with Nanosphere Lithography Platforms" (2012). *Electronic Thesis and Dissertation Repository*. 467.

<https://ir.lib.uwo.ca/etd/467>

This Dissertation/Thesis is brought to you for free and open access by Scholarship@Western. It has been accepted for inclusion in Electronic Thesis and Dissertation Repository by an authorized administrator of Scholarship@Western. For more information, please contact [wlsadmin@uwo.ca](mailto:wlsadmin@uwo.ca).

ENHANCING RAMAN AND FLUORESCENCE SPECTROSCOPIES WITH  
NANOSPHERE LITHOGRAPHY PLATFORMS

(Spine title: Nanosphere Lithography Platforms for Surface Spectroscopy)

(Thesis format: Monograph)

by

Shabila Fayyaz

Graduate Program in Chemistry

A thesis submitted in partial fulfillment  
of the requirements for the degree of  
Master of Science

The School of Graduate and Postdoctoral Studies  
The University of Western Ontario  
London, Ontario, Canada

© Shabila Fayyaz 2012

THE UNIVERSITY OF WESTERN ONTARIO  
School of Graduate and Postdoctoral Studies

**CERTIFICATE OF EXAMINATION**

Supervisor

Examiners

\_\_\_\_\_  
Dr. François Lagugné-Labarthe

\_\_\_\_\_  
Dr. Ron R. Martin

Supervisory Committee

\_\_\_\_\_  
Dr. Oleg Semenikhin

\_\_\_\_\_  
Dr. Lyudmila Goncharova

The thesis by

**Shabila Fayyaz**

entitled:

**Enhancing Raman and Fluorescence Spectroscopies with  
Nanosphere Lithography Platforms**

is accepted in partial fulfillment of the  
requirements for the degree of  
Master of Science

\_\_\_\_\_  
Date

\_\_\_\_\_  
Chair of the Thesis Examination Board

## Abstract

Localized surface plasmon resonance (LSPR) is of particular interest to enhance the limit of detection in spectroscopic techniques such as Raman and fluorescence via a surface enhancement from metallic nanostructures. In this study, using nanosphere lithography (NSL) technique, a series of gold nanostructures over glass surfaces are prepared. These nanostructures are used to record the surface enhanced Raman scattering (SERS) spectra of benzenethiol and azobenzene thiol and the vibrational modes are compared to the literature. Once protected with an ultrathin layer of SiO<sub>2</sub>, the gold nanostructures are investigated using scanning confocal fluorescence microscopy to detect the fluorescence from a dye solution. Herein, we show that the NSL-fabricated nanotriangle arrays made with particle sizes with dimensions closer to the excitation wavelength can be used to study the SERS spectrum of the molecule and, in the case of surface enhanced fluorescence (SEF), display the most intense hot-spots for each bow-tie assembly oriented along the polarization direction of the impinging light.

**Keywords:** Localized surface plasmon resonance (LSPR), nanosphere lithography (NSL), surface enhanced Raman scattering (SERS), surface enhanced fluorescence (SEF), bow-tie assembly, hot-spots

## Co-Authorship Statement

The following thesis contains material from a submitted paper. Dr. François Lagugné-Labarthe was the corresponding author of the paper presented and was responsible for the supervision of Shabila Fayyaz over the course of her studies.

The submitted paper is presented in Chapter 4, Shabila Fayyaz was the first author of this paper responsible for the experimental work and writing and reviewing the draft several times. Some experimental work was jointly done and analyzed with Mohammadali Tabatabaei and he also helped in writing of the manuscript and reviewing it. Shabila highly appreciated his help and useful discussion.

## Acknowledgements

I would take the opportunity to thank my supervisor, Dr. François Lagugné- Labarthe for his guidance and support throughout my research project. I would also like to thank the staff at Western Nanofabrication Facility: Dr. Todd Simpson, Tim Goldhawk and Dr. Rick Glew for many hours of training and Dr. Richard Harris at the Biotron Facility. I would like to thank the present and past members of the Lagugné- Labarthe group: Betty Galaretta, Nastaran Kazemi, Mathew Paul Brockman, Taylor, Farshid, Renjie and Nathan Peter Yundt for their support and friendship. Most importantly, I would like to thank Mohammadali Tabatabaei for his help with some of the experiments and data analysis. I would also like to mention Jan Mathers and Sandra Zakaria Holtslag for making it possible to survive the first year labs.

Outside of the lab, I would extend my thanks to all my friends, especially Faiqua Khalid, for being there whenever I needed her. Finally, I would like to extend my gratitude to Mom, Dad and my sister, Afshan for their constant love and support.

# Table of Contents

<b>CERTIFICATE OF EXAMINATION .....</b>	<b>ii</b>
<b>Abstract.....</b>	<b>iii</b>
<b>Co-Authorship Statement .....</b>	<b>iv</b>
<b>Acknowledgements .....</b>	<b>v</b>
<b>Table of Contents .....</b>	<b>vi</b>
<b>List of Tables .....</b>	<b>x</b>
<b>List of Figures.....</b>	<b>xi</b>
<b>List of Abbreviations .....</b>	<b>xiv</b>
<b>Chapter 1 .....</b>	<b>1</b>
<b>1 General Introduction .....</b>	<b>1</b>
<b>1.1 Raman Spectroscopy .....</b>	<b>1</b>
<b>1.2 Fluorescence Spectroscopy.....</b>	<b>3</b>
<b>1.3 Surface-Enhanced Raman Scattering (SERS) .....</b>	<b>5</b>
1.3.1 Electromagnetic mechanism of SERS .....	5
1.3.2 Chemical Mechanism of Enhancement .....	9
1.3.3 SERS Substrate .....	9
<b>1.4 Surface –Enhanced Fluorescence .....</b>	<b>11</b>
<b>1.5 Techniques for Fabrication of Nanostructures .....</b>	<b>13</b>
1.5.1 Photolithography.....	13
1.5.2 Electron Beam Lithography .....	14
1.5.3 Nanoparticles .....	14
<b>1.6 Fabrication of substrate .....</b>	<b>15</b>
1.6.1 Nanosphere Lithography.....	15

1.6.2	Choice of metal .....	16
<b>1.7</b>	<b>Scope of Thesis .....</b>	<b>17</b>
<b>Chapter 2</b>	<b>.....</b>	<b>19</b>
<b>2</b>	<b>Fabrication of Substrate by Nanosphere Lithography.....</b>	<b>19</b>
<b>2.1</b>	<b>Introduction.....</b>	<b>19</b>
<b>2.2</b>	<b>Materials and Methods.....</b>	<b>24</b>
2.2.1	Reagents .....	24
2.2.2	Cleaning of Glass Slides .....	25
2.2.3	Preparation of Sample by Nanosphere Lithography .....	25
2.2.4	Gold Deposition .....	26
2.2.5	Lift- off.....	28
2.2.6	Surface Characterization of the Samples .....	28
2.2.6.1	Optical Images.....	28
2.2.6.2	Scanning Electron Microscopy (SEM).....	28
2.2.6.3	Atomic Force Microscopy (AFM).....	30
2.2.6.4	Extinction Spectrum .....	31
<b>2.3</b>	<b>Results and Discussion.....</b>	<b>33</b>
2.3.1	Surface Characterization of the Nanotriangle Array .....	33
2.3.1.1	Fabrication of Polystyrene monolayer.....	33
2.3.1.2	Uniformity of the Array.....	35
2.3.1.3	Thickness of gold deposited .....	37
2.3.1.4	LSPR wavelength of nanotriangle arrays.....	39
<b>2.4</b>	<b>Conclusion .....</b>	<b>42</b>



<b>Chapter 3 .....</b>	<b>43</b>
<b>3 Surface Enhanced Raman Spectroscopy .....</b>	<b>43</b>
<b>3.1 Introduction.....</b>	<b>43</b>
<b>3.2 Materials and Methods.....</b>	<b>47</b>
3.2.1 Reagents .....	47
3.2.2 Fabrication of Nanotriangles.....	48
3.2.3 Functionalization of the SERS Platforms .....	48
3.2.4 Raman Spectroscopy.....	48
<b>3.3 Results and Discussion.....</b>	<b>50</b>
3.3.1 Assignment of Raman Spectra of Benzenethiol .....	50
3.3.2 Assignment of Raman spectra of azobenzene thiol .....	53
3.3.3 Effect of different size of nanotriangles on the Raman signal.....	56
<b>3.4 Conclusion .....</b>	<b>57</b>
<b>Chapter 4 .....</b>	<b>58</b>
<b>4 Mapping hot-spots on nanotriangle array using fluorescence microscopy .....</b>	<b>58</b>
<b>4.1 Introduction.....</b>	<b>58</b>
<b>4.2 Materials and Methods.....</b>	<b>62</b>
4.2.1 Reagents .....	62
4.2.2 Fabrication of nanotriangle arrays .....	62
4.2.3 Sputtering of silica on the substrates .....	62
4.2.4 Imaging the Samples.....	64
4.2.4.1 Focused ion beam- Scanning electron microscopy (FIB-SEM). 64	
4.2.4.2 Confocal Fluorescence Microscopy .....	65
<b>4.3 Results and Discussion.....</b>	<b>68</b>
4.3.1 Fabrication of Gold Nanotriangle arrays .....	68

4.3.2	Size dependency of nanotriangles on fluorescence enhancement .....	71
4.3.3	Effect of SiO <sub>2</sub> thickness on fluorescence enhancement.....	78
<b>4.4</b>	<b>Conclusion .....</b>	<b>80</b>
<b>Chapter 5</b>	<b>.....</b>	<b>81</b>
<b>5</b>	<b>Summary and Future Prospectives .....</b>	<b>81</b>
5.1	Summary.....	81
5.2	Future Prospects .....	83
5.3	References.....	87
<b>Curriculum Vitae</b>	<b>.....</b>	<b>99</b>

## List of Tables

<b>Table 2-1</b> Height and the distance between nanotriangles given in each case.....	36
<b>Table 3-1</b> Assignment of vibrational modes for benzenethiol .....	52
<b>Table 3-2</b> Assignment of vibrational modes for azobenzene thiol molecule.....	54

## List of Figures

<b>Figure 1-1</b> Model for illustration of Stokes, Rayleigh and anti-Stokes scattering.....	2
<b>Figure 1-2</b> Illustration of the fluorescence process.....	4
<b>Figure 1-3</b> Schematic illustrating a localized surface plasmon <sup>17</sup> .....	6
<b>Figure 2-1</b> Illustration of the nanotriangle array obtained and the representation of $d_{ip}$ (interparticle distance) and $a$ (perpendicular bisector of triangle) .....	22
<b>Figure 2-2</b> Schematic illustration of sample at various stages: a) top view of polystyrene nanospheres on glass slide, b) deposition of Au, c) top view of nanotriangles after removing polystyrene particles, d) side view of nanotriangles after particle removal .....	26
<b>Figure 2-3</b> Electron beam evaporation of gold on the sample <sup>83</sup> .....	27
<b>Figure 2-4</b> Schematic diagram of a scanning electron microscope with CRT display <sup>85</sup> .....	29
<b>Figure 2-5</b> A simplified schematic diagram of the basic setup and main components of the AFM; the laser deflection off the cantilever is directed onto the photodiode after the tip encounters a surface feature <sup>86</sup> .....	30
<b>Figure 2-6</b> Schematic of the extinction spectra setup .....	32
<b>Figure 2-7</b> Optical images objective 100x (N.A. 0.95) a) sample with polystyrene particles, 1.00 $\mu\text{m}$ , b) same sample after gold deposition and lift –off of particles .....	35
<b>Figure 2-8</b> SEM images of a) 0.43 $\mu\text{m}$ b) 0.65 $\mu\text{m}$ c) 1.00 $\mu\text{m}$ gold nanotriangle arrays and monolayer of polystyrene nanospheres showed in right bottom corners.....	37
<b>Figure 2-9</b> AFM image (5x5 $\mu\text{m}$ ) a) polystyrene particles coated with gold (0.43 $\mu\text{m}$ ), b) nanotriangles array after the lift- off.....	38
<b>Figure 2-10</b> Typical extinction spectra of 0.43, 0.65 and 1.00 $\mu\text{m}$ nanotriangle sample .....	41

<b>Figure 3-1</b> Schematic of confocal Raman spectrometer showing the main components .....	49
<b>Figure 3-2</b> Structure of benzenethiol (BT).....	51
<b>Figure 3-3</b> Raman spectra of benzenethiol on nanotriangle sample .....	52
<b>Figure 3-4</b> Structure of azobenzene thiol.....	53
<b>Figure 3-5</b> Raman spectra of azobenzene thiol on nanotriangle sample.....	54
<b>Figure 3-6</b> Photoisomerization reaction of azobenzene thiol molecule when irradiated.....	55
<b>Figure 4-1</b> Schematic diagram of the operation of a magnetron sputtering system, a) Argon atoms enter the system and collide with electrons; b) Argon atoms become ionized; c) Ar ions collide with the target surface; d) Target atoms are removed from the surface; e) Target molecules adhere to the substrate surface.....	64
<b>Figure 4-2</b> A simplified diagram of the light pathways and important components of the confocal microscope <sup>144</sup> .....	67
<b>Figure 4-3</b> Schematic illustration of experimental procedure; a) top view of polystyrene nanospheres on glass slide, b) deposition of Au, c) top view of nanotriangles after removing polystyrene particles, d) SiO <sub>2</sub> sputtering, e) side view of prepared substrate on coverslip; yellow layer: Au; gray layer: SiO <sub>2</sub> , f) adding a drop of dye (IRIS5 10 μM) on sample and exciting with He-Ne Laser (632.8 nm) for fluorescence measurement .....	69
<b>Figure 4-4</b> a) SEM image of NSL platform made with 1.00 μm polystyrene nanospheres b) SEM image of the cross-section of a nanotriangle milled using focused ion beam with 20 nm of SiO <sub>2</sub> deposited on top c) The same SEM-FIB image as “b” with higher magnification ..	70
<b>Figure 4-5</b> Fluorescence images showing individual “hot-spots” on GNT arrays after adding the dye: a) 0.43 μm b) 0.65 μm c) 1.00 μm .....	72
<b>Figure 4-6</b> Illustration of: a) the model of GNT arrays before adding the dye, b) the model of individual hot-spots after adding the dye, c) fluorescence image of 0.65 μm GNT arrays with 25 nm silica on top before adding the dye, d) mapping individual hot-spots after adding the dye on the same fluorescence image demonstrated in c .....	74

**Figure 4-7** a) SEM image of 0.43  $\mu\text{m}$  polystyrene monolayer, b) fluorescence image of GNT arrays (II) along with 0.43 nanospheres (I) without dye, c) fluorescence image of GNT arrays (II) along with 0.43 nanospheres (I) with dye..... 77

**Figure 4-8** The lens effect when the incoming light is focused on to the polystyrene nanospheres..... 78

**Figure 5-1** Fluorescent image of a myoblast cell cultured in single cell patterning <sup>160</sup> ..... 84

**Figure 5-2** a) Optical image of fluoropolymer patterned substrate with polystyrene nanospheres (1.00  $\mu\text{m}$ ) taken with 100 x objective (N.A.0.95), b) optical image taken with 20x objective (N.A.0.5) of the same substrate followed by gold deposition and then lift-off 85

## List of Abbreviations

AFM	atomic force microscopy
BT	benzenethiol
CCD	charged coupled device
FIB-SEM	focused ion beam-scanning electron microscopy
GNT	gold nanotriangles
LSPR	localized surface plasmon resonance
NSL	nanosphere lithography
SAM	self- assembled monolayer
SEF	surface enhanced fluorescence
SEM	scanning electron microscopy
SERS	surface enhanced Raman spectroscopy
SHINERS	shell isolated nanoparticle enhanced Raman spectroscopy
SHINEF	shell isolated nanoparticle enhanced fluorescence
SPR	surface plasmon resonance
TERS	tip enhanced Raman spectroscopy

## Chapter 1

### 1 General Introduction

In order to gain a more complete understanding of the research described in this thesis, a brief introduction about Raman and fluorescence spectroscopies is discussed. Following this, the mechanisms involved in the enhancement of these signals is presented in detail. Thereafter various lithography techniques used for making the substrates for applications in enhanced spectroscopies are discussed. Finally, the scope of the thesis is discussed.

#### 1.1 Raman Spectroscopy

Raman spectroscopy is a valuable technique for chemical and biological analysis as it provides information about molecular structures, surface processes and interface reactions.<sup>1</sup> Raman scattering is generally less widely used than other techniques, due to inherently weak signal but recent developments such as highly efficient detectors or the ways to increase Raman signal make it an attractive technique for vibrational measurements.<sup>2,3</sup>

When a light source impinges matter it can interact with atoms and molecules in several ways. Briefly, light can be absorbed if it matches the electronic or vibrational energy levels of the sample or it can be scattered. In Raman spectroscopy two types of scattering are identified. The most intense form of scattering is Rayleigh scattering which occurs when electron cloud relaxes and no change in energy is observed as this is an



elastic process. Thus, when light is scattered from a molecule most photons are elastically scattered and the scattered photons have same wavelength as the incident photon. However, a very small amount of light, 1 photon for  $10^8$  incident photons, is scattered at frequencies different than the incident light. This process leads to inelastic scattering which is also known as the Raman effect, which occurs when the light and the electron interact that resulting in inelastic scattering of light. The scattered light with lower-energy as compared to the incident laser light is called Raman Stokes scattering and the radiation with higher energy is referred to Raman anti-Stokes scattering.

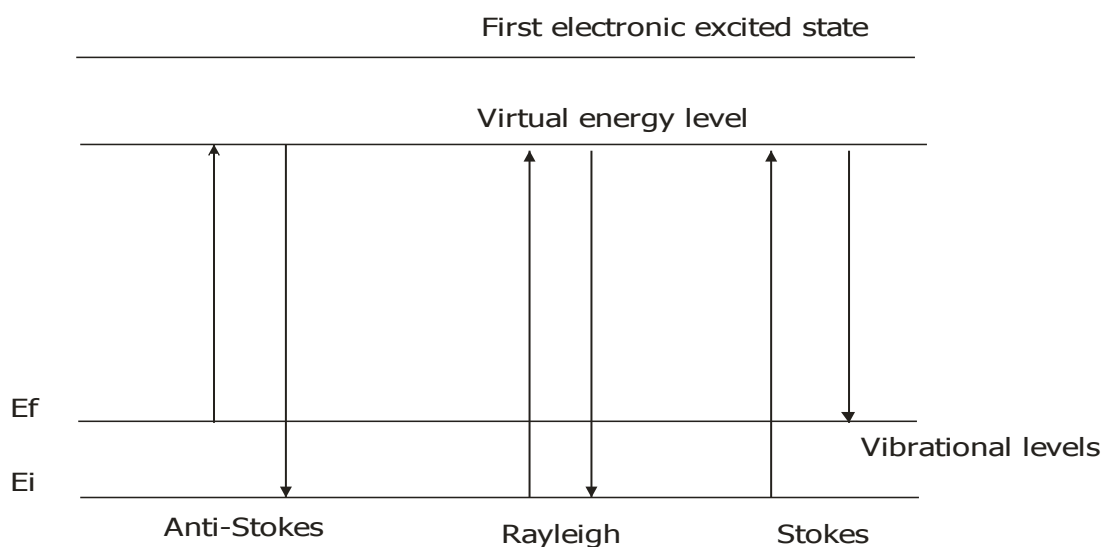


**Figure 1-1** Model for illustration of Stokes, Rayleigh and anti-Stokes scattering

In Figure 1-1, the model of elastic light scattering (Rayleigh) and inelastic light scattering (Stokes and anti-Stokes) processes are depicted.  $E_f$  and  $E_i$  represent the adjacent vibrational levels in a system. A photon of energy is incident on the system: the Stokes-Raman effect results from transition from lower energy level ( $E_i$ ) to higher energy

level ( $E_f$ ) – through a virtual energy level, the energy of which is smaller than the first excited electronic state. The anti-Stokes effect corresponds to a transition from higher energy level ( $E_f$ ) to a lower one ( $E_i$ ) also through an intermediate virtual energy level. The anti-Stokes process is less intense than the Stokes intensity as the anti-Stokes scattering occurs from an excited state ( $E_f$ ), which is less populated than the ground state ( $E_i$ ) at room temperature, according to the Boltzmann distribution. Thus, in most cases Raman measurements implies the detection of the Stokes-shifted scattering.<sup>2,3</sup>

## 1.2 Fluorescence Spectroscopy

Fluorescence spectroscopy is of great interest due to the widespread fluorescence based applications in the field of chemistry, molecular biology, photonics and materials science.<sup>4</sup> The Jablonski diagram (Figure 1-2) depicts nicely the different optical processes involving radiative and non-radiative decays: photon absorption, internal conversion and fluorescence. In this diagram, the singlet state is denoted by  $S_0$  (ground electronic state),  $S_1$ ,  $S_2$ ,.... . It is important to note that absorption is very fast while lifetime of fluorescence is approximately  $10^{-10}$ - $10^{-7}$ s with respect to other processes. Absorption of a photon can bring a molecule to one of the vibrational levels of  $S_1$ ,  $S_2$ ,.... Internal conversion is a non-radiative transition between two electronic states. This process is followed by vibrational relaxation towards the lowest vibrational level in the same electronic level. Fluorescence is a two step process consisting of absorption of a photon, followed by spontaneous emission (SE) from  $S_1$ - $S_0$  relaxation. The fluorescence spectrum is located at higher wavelength (lower energy) than the absorption spectrum because of

the energy loss in the excited state due to vibrational relaxation. The emission process occurs at a longer wavelength as compared to absorption. After the excitation of a population of molecules by a very short pulse of light, the fluorescence intensity decreases exponentially with the characteristic time, reflecting the average lifetime of the molecules in the  $S_1$  excited state.<sup>5</sup>

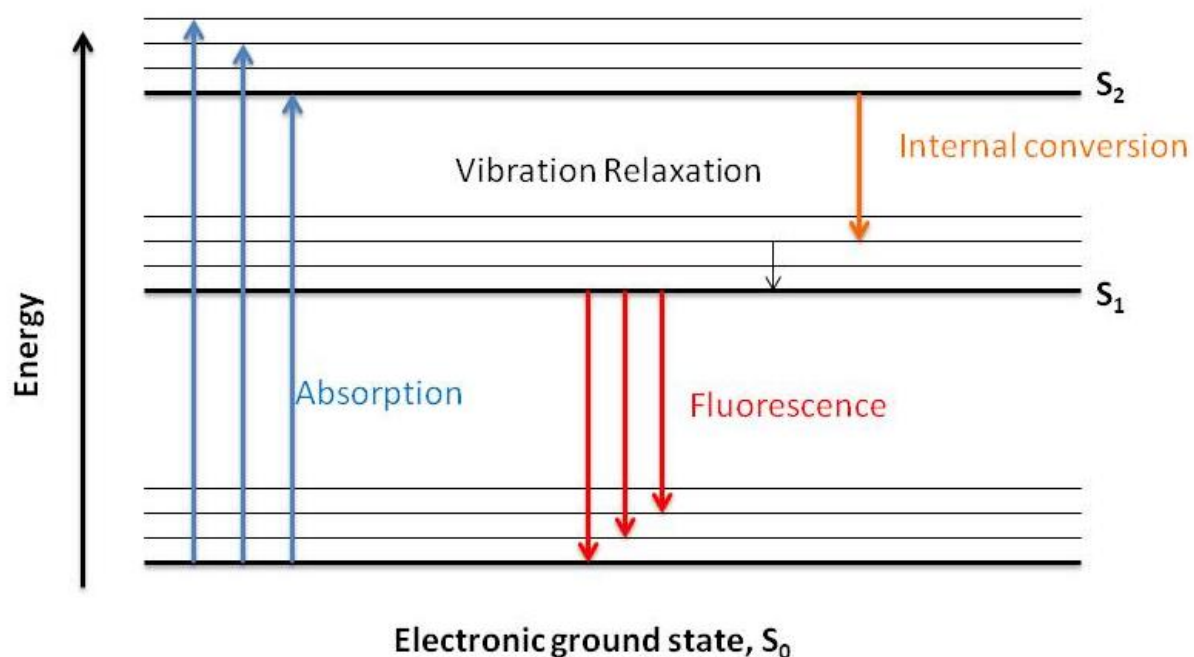


**Figure 1-2** Illustration of the fluorescence process

## 1.3 Surface-Enhanced Raman Scattering (SERS)

Since its observation by Fleischmann et al. in 1974<sup>6</sup>, SERS has matured into a widely used analytical tool for microscopy and spectroscopy.<sup>2, 7</sup> It is an ultra-sensitive technique for the detection of molecules on or nearby the surface of metallic nanostructures which can support localized surface plasmon resonance (SERS substrate).<sup>8, 9</sup> The signal levels observed in SERS is around six to eight orders of magnitude higher than in conventional Raman, providing sensitivity required for bio-analytical and biomedical applications.<sup>8, 9</sup> SERS effect is generally considered to arise from the electromagnetic effect and the chemical effect, but the former mechanism plays a vital role in enhancing the Raman signal. The inelastic Raman scattering is proportional to the square of the polarizability and the electric field. Consequently, if the local electric field is increased by a surface effect, the value of its square will also be increased greatly resulting in an enhanced SERS signal.<sup>5</sup> The maximum SERS enhancement occurs in hot spots, which refers to a confined region with dimensions of the order of less than 10-100nm<sup>10</sup> between two metallic nanoparticle, where the surface plasmon of the metal nanoparticles can be coupled to each other to produce more intense electromagnetic fields.<sup>11</sup>

### 1.3.1 Electromagnetic mechanism of SERS

The interesting optical attributes of metal nanoparticles, as reflected in their bright intense colors, are due to their unique interaction with light. In the presence of the oscillating electromagnetic field of the light the free electrons of the metal nanoparticle undergo a collective coherent oscillation with respect to positive metallic lattice. This

process is resonant at a particular frequency of light and it is termed as a localized surface plasmon resonance (LSPR) oscillation. This results in selective absorption of photons of light and generation of a locally enhanced electromagnetic field. The LSPR can be tuned by changing the size, the shape, the composition or the environment of the nanostructure.<sup>12-16</sup>

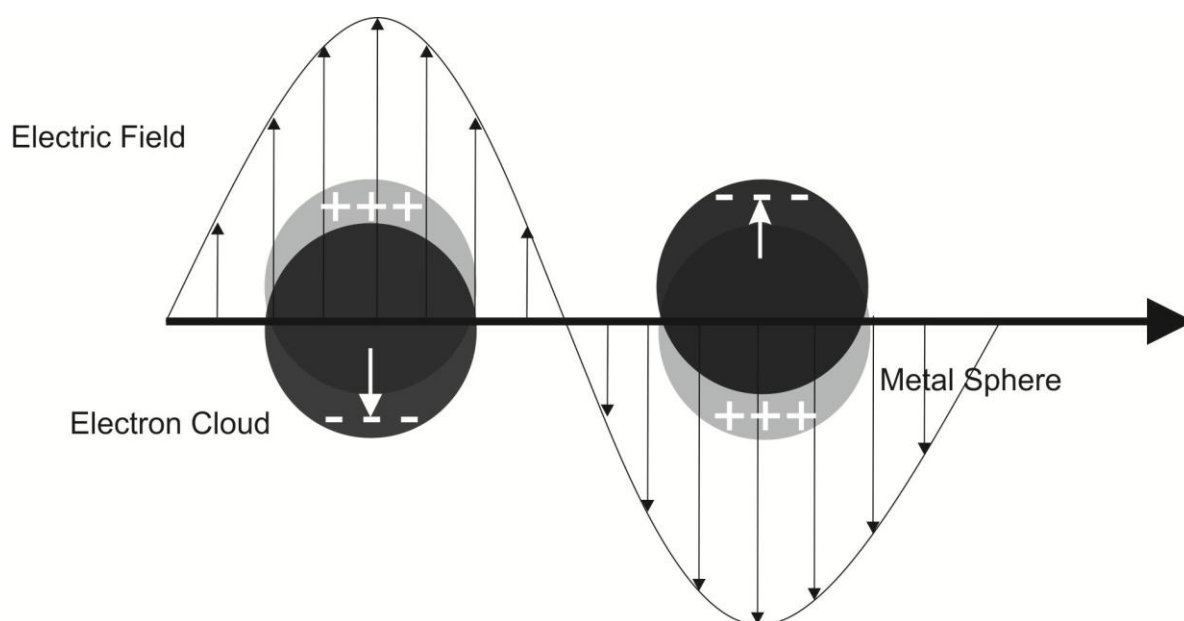


**Figure 1-3** Schematic illustrating a localized surface plasmon<sup>17</sup>

A small metal sphere with dimensions smaller than the wavelength of illuminating light will sustain oscillating surface plasmon multipoles of various order induced by the time varying electric field vector of the light. Systems with free or almost free electrons will sustain such excitations; and the freer the electrons, the sharper and more intense the LSPR. When the exciting laser is resonant with the LSPR, the metal particle will radiate light characteristic of dipolar radiation. This radiation is a coherent process with the

exciting field and is characterized by a spatial distribution of field magnitudes in which the light intensity from a certain portion of the space surrounding the particle is depleted while the intensity at certain portions near the metal particle is enhanced. The field enhancement averaged over the surface of the particle is,  $g$ , and the average magnitude of the field radiated by the metal particle,  $E_s$ , will be:

$$E_s = gE_0 \quad (1.1)$$

where  $E_0$  is the magnitude of the incident field. The molecule adsorbed on the surface of the metal particle will be excited by local near field at the particle surface  $E_s$ , and the Raman scattered light produced by the molecule will have a field strength  $E_R$ , which is given by following equation:

$$E_R \propto \alpha_R E_s \propto \alpha_R g E_0 \quad (1.2)$$

where  $\alpha_R$  is appropriate combination of components of the Raman polarizability. The Raman-scattered field can be enhanced further by metallic particle in the same way as the incident field was, i.e. the metallic particle can scatter light at the Raman shifted wavelength enhanced by  $g'$  thus the amplitude of the SERS-scattered field will be given by :

$$E_{SERS} = \alpha_R g g' E_0 \quad (1.3)$$

The average SERS intensity will be proportional to the square modulus of  $E_{SERS}$ , i.e.,

$$I_{SERS} = |\alpha_R|^2 |g g'|^2 I_0 \quad (1.4)$$

where  $I_{\text{SERS}}$  and  $I_0$  are intensities of the SERS scattered and incident light respectively. For low wavenumber bands, i.e.  $g \sim g'$ , SERS intensity will be enhanced by the factor proportional to the fourth power of enhancement of the local incident near field. Thus, the nanoparticle acts as an antenna efficiently amplifying the Raman signal. For Raman modes at higher wavenumber, the SERS intensity will be more complicated function of plasmon resonant properties of the metallic particle according to the precise wavelength at which incident and Raman scattered light falls. Thus, it is helpful to define SERS enhancement,  $G$ , as a ratio of the Raman-scattered intensity in the presence of the metallic particle to its value in absence of the metallic particle:

$$G = \left| \frac{\alpha_R}{\alpha_{R_0}} \right| |g g'|^2 \quad (1.5)$$

where  $\alpha_{R_0}$  is the Raman polarizability of the isolated molecule.<sup>17-19</sup> In theory, the proportionality between the field strength of the LSPR irradiation and incoming field shows that extremely high Raman scattering intensities of molecules close to the surface can be achieved.<sup>20</sup> This strong distance dependence leads to the observed surface selectivity in SERS: the molecules close to nanoparticle surface experience enormous field enhancement. The orientation of the adsorbed molecule influences the SERS signal therefore adsorption of the molecule of interest is the key step for SERS.<sup>21</sup>

### 1.3.2 Chemical Mechanism of Enhancement

Although electromagnetic model can explain important features of SERS effect, secondary sources of enhancement are also involved. The chemical nature of the enhancement is of importance and this whole enhancement mechanism involves chemisorption of the molecule onto the metal surface. This allows the charge transfer (electrons or holes) from metal surface into the molecule increasing the polarizability of the molecule.

The enhancement is thought to proceed via the new electronic states that are produced due the formation of a bond between the metal surface and molecule. These states are thought to be resonant intermediates during Raman scattering. Thus, as opposed to radiation being absorbed or scattered through plasmons on the surface, the radiation is absorbed into the metal that results in the formation of a hole due to the displacement of an electron from the metal atom. A hole is transferred into the adsorbate metal atom cluster, the Raman process then occurs, excitation is transferred back into the metal and re-radiation occurs from the metal surface. The chemical enhancement is observed only from molecules directly attached to the surface and consequently increases up to monolayer coverage.<sup>1, 22, 23</sup>

### 1.3.3 SERS Substrate

In order for SERS substrate to be suitable for various applications it must be reproducible, stable over the duration of the experiment, should have low cost, should be easy to prepare, non-toxic and chemically compatible with the molecules to be detected.<sup>24</sup> SERS enhancement arises from the resonant response of the substrate which is wavelength dependent. Most SERS substrates are designed to work in the visible or near-



infrared excitation (400-1000 nm), which is usually the range for a Raman experiment. A larger surface area increases the potential number of molecules which can produce SERS.<sup>5</sup>

If the SERS signal of a molecule is low then the following options can be used to overcome this problem: to increase the substrate surface area or to increase the laser power. The condition for the molecule to be a good Raman scatterer is not enough but it must be able to adsorb efficiently on the SERS substrate. Some molecules have a strong chemical affinity for the metal surface and are easier to work with such as thiol<sup>25</sup> or triazole.<sup>26</sup> Another common mechanism for attachment of a molecule to the metallic nanostructure is through electrostatic interaction.<sup>5, 27</sup>

Various factors affect the working wavelength of the SERS substrate such as size, shape of metallic nanostructures and gap between two nanostructures. As the size of the nanoparticles increases so the LSPR is red shifted to longer wavelength and it is broadened due to the damping effect (energy lost through scattering).<sup>16, 28</sup>

The shape of the nanoparticles has a strong influence on the LSPR of the substrate. For nanostructures with flat surface as compared to spheres, the resonance wavelength is blue shifted but in the case of nanostructures with sharp surface, the resonance wavelength is red shifted as compared to the LSPR of the spheres.<sup>29, 30</sup> The interaction between two nanostructures (small gap) results in large local field enhancement resulting in hot-spot.<sup>31</sup> The supporting substrate can also have dramatic influence for the electromagnetic response of the nanoparticles but, this point is not really considered in the present work since our substrate is made of amorphous glass. In other work, the

LSPR of silver nanoparticles is around 520 nm while upon introduction of the substrate it red shifts to 620 nm.<sup>32</sup>

The ratio of the surface-enhanced Raman scattering (SERS) intensity per adsorbed molecule to the normal Raman scattering per bulk molecule is defined as the enhancement factor (EF) and quantifies the enhancing capability of a SERS-active structure.<sup>33</sup> The magnitude of the enhancement factor (EF) is the most crucial step of SERS but enhancement is not straightforward to measure as the main difficulties lies in the estimation of the number of molecules on SERS substrate. The maximum SERS EF occurs at the specific positions on the surface (resulting in hot-spots) and maximum SERS EF can be  $10^6$  on the spherical nanoparticle and can be as high as  $10^{10}$ - $10^{11}$  at the apex of the metallic nanotriangles.<sup>5</sup>

## 1.4 Surface –Enhanced Fluorescence

The theory of surface-enhanced fluorescence was developed extensively in the 1970-1980.<sup>34</sup> However, it has only recently been observed experimentally so that these theories can be confirmed.<sup>35-37</sup> SEF consists of a modification of the fluorescence intensities and lifetimes for the molecules absorbed on (or by few nanometers) a metal surface.<sup>5</sup> The presence of a shell coated nanoparticle can reduce the lifetime of the excited state of the fluorophore thus resulting in the quenching of fluorescence faster.<sup>38</sup> This arises from the strong electromagnetic (EM) response of the metallic objects, particularly localized surface plasmon are excited.<sup>5</sup>

A large quenching or enhancement of the fluorescence can be observed depending on the exact conditions and this can be understood by electromagnetic theory.<sup>34</sup> Fluorescence is very similar to scattering; it involves the adsorption of a photon, followed by emission. The same enhancement mechanisms as that derived for SERS are therefore expected. The crucial difference is that scattering (SERS) is instantaneous, while fluorescence is a multi- step process. This means that for SERS, both enhancements (local field and radiative) contribute to the SERS cross-section.<sup>5</sup>

For fluorescence, the local field enhancement leads to modification of absorption cross-section, but the radiative enhancements only lead to modification of the decay rates (radiative and non-radiative), which compete with each other.<sup>5</sup> Surface plasmon are electron plasma oscillations near a metal surface which is perpendicular to the metal surface. The charge oscillations are orthogonal to the surface plane and this induces an evanescent electromagnetic field. The combined surface plasmon and induced photon is called surface plasmon- polariton (SPP). The coupling between the propagative light and SPP helps in excitation and enhancement of the emission process.<sup>39</sup> A good agreement between the theoretical explanation of the fluorescence enhancement and the experimental results is found for metal-fluorophore distances larger than 10 nm. The spacer layer causes an increase in relaxation rate, which allows it to undergo more excitation–emission cycles before photobleaching.<sup>40</sup>

There are other situations where the modification of the fluorescence spectrum is known to occur. This includes: formation of dye aggregates,<sup>41</sup> a chemical modification of dye properties upon adsorption on a metal surface<sup>42</sup> and a shift of the fluorophore energy levels as a result of electromagnetic interactions.<sup>43, 44</sup> When the fluorophores are

immobilized on a transparent substrate such as glass or fused silica, the presence of interface induces small changes in their emission properties.<sup>40</sup>

## 1.5 Techniques for Fabrication of Nanostructures

Nanofabrication is any process which generates patterns of structures with size less than 100nm in one of the dimension. There are two strategies to obtain material in nanoscale: bottom-up method where atoms are assembled to generate nanostructures or top-down method where material is removed from bulk material leaving the desired nanostructure. Common top-down techniques are electron beam lithography (EBL) and photolithography which suffer from the need to remove large amounts of material and are expensive fabrication techniques while bottom-up technique lacks uniformity. Examples of bottom-up techniques are nanosphere lithography and synthesis techniques.<sup>45, 46</sup>

### 1.5.1 Photolithography

Photolithography is perhaps the most widely used microfabrication technique. It produces patterned features that can be precisely controlled down to micron dimension.<sup>47</sup> This method is used to transfer a pattern that is drawn on a photomask to a substrate by UV radiation of a photo-sensitive polymer called a photoresist. The photoresist is first spin coated on the surface of a substrate to create a thin film, and is then brought into contact with the mask. The ultraviolet (UV) source is activated and illuminates the exposed areas of the photoresist, which is then removed by a solvent, creating patterned structures of photoresist, and windows that provide access to the underlying substrate for

further modifications. The photoresist features can be used as a lift-off mask for patterning chemical species.<sup>48, 49</sup> Nanostructures produced on silicon wafer using photolithography have been used to study the SERS spectrum of glucose.<sup>50</sup> It has been reported that 3-dimensional nanoarrays made by photolithography were used to record the SERS spectra of Rhodamine 6G.<sup>51</sup>

### 1.5.2 Electron Beam Lithography

Electron beam lithography is based on the same principle that some macromolecule polymers are sensitive to electrons and the polymer can be patterned by electron beam exposure. The electron resists are similar to photoresists so the exposure of this resists is the same process as that of the photon exposure of the photoresists but the only difference is its higher resolution. It is apparent that higher the electron energy shorter the wavelength. It is a versatile micro-patterning technique with lots of applications. While patterning by optical lithography can only be done through photomasks, electron beam can directly expose and pattern on the resist.<sup>47</sup>

### 1.5.3 Nanoparticles

Methods have long been known to generate colored glass by adding gold nanoparticles to generate burgundy, red or purple colors. Faraday attributed this color to finely divided colloidal gold nanoparticles. As the size and the shape changes consequently the color of solution also changes. It is found that this color is due to the collective oscillation of the electrons in the conduction band known as surface plasmon

oscillation. The oscillation frequency for gold and silver is in the visible region. Metal nanoparticles generate enhanced electromagnetic fields which affect the local environment. The field is determined by the geometry of the nanoparticle and enhances fluorescence or the Raman signal of the molecule on the surface. The synthesis of nanoparticles requires the use of capping materials such as surfactant or polymer to prevent aggregation and precipitation of the nanoparticles. The choice of reduction technique, time and capping material determines the size and shape of the nanoparticles.<sup>46</sup> El -Sayed and coworkers have used conjugated gold nanoparticles to study the SERS spectrum of the cancer cells.<sup>52</sup> Bardhan and coworkers have reported the fluorescence enhancement using gold nanoshells and nanorods with the fluorescent molecule complex.<sup>53</sup>

## 1.6 Fabrication of substrate

The substrates for applications in Raman and fluorescence spectroscopies were fabricated by nanosphere lithography followed by deposition of gold and then lift- off.

### 1.6.1 Nanosphere Lithography

Nanosphere lithography is a technique which involves the self-assembling hexagonal monolayer of polymer spheres used as a shadow mask for subsequent metal deposition followed by the removal of nanosphere mask. This has been successfully used to produce large arrays of gold nanoparticles and triangles. For the strongest plasmonic

coupling it is necessary to control the distance between nanotriangles to only a few nanometers.<sup>54</sup> This technique is discussed in detail in chapter 2.

### 1.6.2 Choice of metal

As described previously, the size of the metal features must be smaller with respect to the exciting wavelength for surface enhanced processes to occur; this means the nanostructures must possess size in the range of 5-100 nm. If the size of the nanostructure is smaller than the wavelength of the incident light then the electronic scattering processes disappear at the particle surface.<sup>18</sup>

All metals do not exhibit the plasmonic properties but they display a metallic behavior. In most cases, the plasma frequency ( $\omega_p$ ) of metals is observed in the UV region, only the plasma frequency of gold, copper and silver lie in the visible region which is also the region of interest since lasers sources used in Raman and fluorescence spectroscopy are often visible sources. Gold and copper are also suitable for longer wavelength typically more than 600nm but copper cannot be used as it easily gets oxidized. Silver and gold are widely used metals in plasmonic application. Gold is preferred over silver for excitation wavelength in the red spectrum (typically 632.8nm) as it has good biocompatibility and stability under the atmospheric conditions.<sup>5, 18</sup> Silver is used when the excitation wavelength is in the green region but as it gets oxidized, it must be used rapidly (i.e. within a day) after the metal deposition.

## 1.7 Scope of Thesis

One research area developed in our group, concerns the fabrication of substrates for surface enhanced Raman and surface enhanced fluorescence spectroscopies (SERS and SEF respectively). Various substrates such as nanoparticles, substrate made by e-beam lithography or photolithography, to enhance the Raman or fluorescence signal have been reported over the last few years as shown in the abundant literature on this topic with applications ranging from sensing bio-toxins to traces of explosive.<sup>55, 56</sup> These substrates lack reproducibility, have high sample cost and low sample throughput. Nanosphere lithography was developed as an alternative strategy. This technique has various advantages such as it is inexpensive, has high throughput and it doesn't require special equipment.<sup>13</sup>

In this thesis, nanosphere lithography was used to fabricate the substrates with varying interparticle size and height of the nanotriangle by using different diameter of polystyrene microspheres. This is followed by metallic gold deposition and then lift-off. These substrates need to be transparent so that they can be used under confocal microscope.

Thus, in Chapter 2, the fabrication of the substrates using nanosphere lithography followed by gold deposition and lift-off. The samples are characterized using SEM and AFM. The working wavelength of the samples was also determined by recording the extinction spectra.



The efficiency of the substrate as a SERS active substrate is explored in Chapter 3, by collecting the SERS spectrum of benzenethiol and azobenzene thiol. In Chapter 4, these substrates are efficiently used to enhance the fluorescence of Iris-5 dye followed by silica deposition. Finally closing remarks and promising applications are discussed in Chapter 5.

## Chapter 2

### 2 Fabrication of Substrate by Nanosphere Lithography

This chapter describes the concept of nanosphere lithography which is used to fabricate nanostructured surfaces. The materials and the preparation method samples have been described extensively. Finally, the results concerning the characterization of the samples prepared are presented and are discussed.

#### 2.1 Introduction

Several standard lithographic methods are commonly used to fabricate nanostructures with controlled size, shape and geometry spacing. One of the most widely used is photolithography,<sup>12, 57</sup> however, it has not been widely applied to nanostructure fabrication as a consequence of its diffraction limited resolution of the features with dimensions in the order of 300nm. Electron beam lithography<sup>12, 58</sup> offers an excellent control of the feature dimensions and shapes with a resolution down to 20nm but to the detriment of low sample throughput and high sample cost.<sup>13</sup> Consequently, several alternatives opening the possibility of parallel nanolithography have been explored and include (1) diffusion controlled aggregation at the surface,<sup>59-61</sup> (2) laser focused atom deposition,<sup>62</sup> (3) chemical synthesis of the metal cluster compounds and semi-conductor nanocrystals,<sup>13</sup> and (4) natural lithography.<sup>63, 64</sup>

The concept of natural lithography was introduced by Fischer and Zingsheim in 1981 when they were working on naturally assembled polystyrene latex nanospheres as a mask for contact imaging of photoresist with visible light.<sup>64</sup> Nanosphere lithography was later extended by demonstrating that a self-assembled nanosphere monolayer could be used as a mask by Deckman and coworkers in 1982.<sup>63</sup> Later, the term nanosphere lithography was coined and it was used by the research group of Van Duyne et al. for applications in spectroscopy.<sup>32, 65</sup>

The resulting two dimensional (2D) colloidal crystals or colloidal monolayer generated from nanosphere lithography have shown to be particularly important to nanoscale surface patterning, which is a key platform for variety of applications such as photonics,<sup>66</sup> biosensors<sup>65</sup> and catalysis.<sup>67</sup> Furthermore, colloidal monolayer surface patterning, i.e. nanosphere lithography,<sup>68</sup> presents a simple and cost effective method of producing symmetric patterns with structural features down to the sub-100 nm regime.<sup>69,</sup>  
<sup>70</sup> There are several advantages of this technique. First, the assembly process takes only a few minutes to prepare the platform which is much faster than using the conventional nanofabrication techniques that involves many delicate steps. Second, large area of colloidal monolayers can be produced without any special apparatus and only small amount of colloidal suspension is required for each experiment. Finally, the 2D colloidal spheres can be transferred to any kind of substrate regardless of surface wettability and smoothness.<sup>71</sup>

Various methods are reported for the deposition of a nanosphere solution onto a desired substrate such as spin coating,<sup>68, 72, 73</sup> the Langmuir-Blodgett technique<sup>74</sup> and air-water transfer.<sup>75</sup> Spin coating is an extremely rapid and simple fabrication method, but

the strong rotational force and its radial gradient hinders the formation of the large, single crystalline domains. Additionally, careful adjustments of concentration, rotational speed and surface functionality have to be carried out for each particle. In the Langmuir-Blodgett technique, the particles are floating over the water surface compressed by a barrier to a packed monolayer and finally transferred on the receiving substrate.<sup>73</sup> In the case of air–water transfer of particles, a drop of surfactant is used to arrange spheres into a monolayer and then a substrate is placed below to lift the monolayer from the surface of the water. In this way, a monolayer of spheres is transferred onto the substrate.<sup>76</sup>

The hydrophobicity of the colloidal particles allows them to float in the air-water interface.<sup>77</sup> However, purely hydrophobic, uncharged particles would not crystallize in a hexagonally close packed geometry; instead these would aggregate in a disordered layer upon contact with the air-water interface. The electrostatic repulsion provides the required mobility for ordered formation before particle aggregation occurs.<sup>73</sup> All of these deposition methods require that the nanospheres are able to diffuse freely across the substrate, seeking their lowest energy configuration. This is often achieved by chemically modifying the nanosphere surface with a negatively charged functional group such as the carboxylate or sulfate that is electrostatically repelled by the negatively charged glass surface. As the solvent evaporates, capillary forces draw the nanospheres together and these crystallize in a hexagonally close- packed pattern on the substrate. Following the self assembly of this mask formed by nanosphere monolayer, a metal is deposited by e-beam evaporation from a source normal to the substrate through the nanosphere mask to a controlled thickness  $d_m$ .

The nanosphere mask is further removed by sonicating the entire sample in a solvent leaving behind the metal deposited through the mask to the substrate. When a metal layer is deposited through the monolayer mask, the interstices between the particles allow deposited metal to reach the substrate, creating an array of triangularly shaped nanoparticles.<sup>13</sup> Figure 2-1 shows the illustration of the nanotriangle array obtained from this technique and the representation of  $d_{ip}$  and  $a$  in the array. Simple geometric calculations define the relationship between the perpendicular bisector of the triangular nanoparticles,  $a$ , and the interparticle spacing,  $d_{ip}$ , to the nanosphere diameter,  $D$ :<sup>13</sup>

$$a = \frac{3}{2} \left( \sqrt{3} - 1 - \frac{1}{\sqrt{3}} \right) D \quad (2.1)$$

$$d_{ip} = \frac{1}{\sqrt{3}} D \quad (2.2)$$

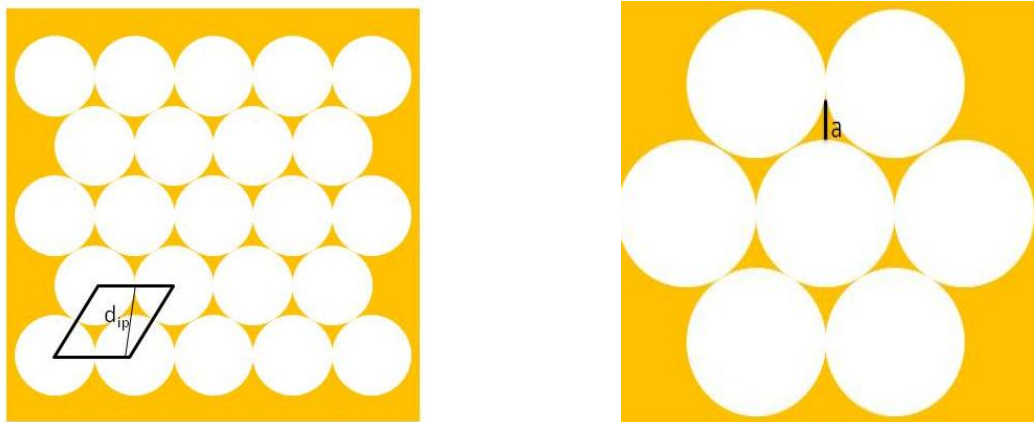


**Figure 2-1** Illustration of the nanotriangle array obtained and the representation of  $d_{ip}$  (interparticle distance) and  $a$  (perpendicular bisector of triangle)

It is noteworthy that Van Duyne's group reported that a double layer periodic polystyrene particle could be formed when the concentration of nanospheres in the solution to be self assembled is increased. When a second layer of nanospheres assembles on to the first, every other three- fold hole is blocked resulting in a regular pattern of hexagonal nanoparticles but smaller in size.<sup>13</sup> In the case of the triangular nanostructures, the aspect ratio (thickness to width) determines the excitation wavelength and ultimately the sensitivity of the plasmonic sensor for a given wavelength.<sup>13, 75</sup> The aspect ratio is dependent on the size of the nanosphere and thickness of the deposited metallic film.<sup>75</sup>

Recently, different structures such as nano-rings,<sup>13</sup> nano-nets,<sup>78</sup> nano-pillars,<sup>79</sup> nanopores,<sup>80</sup> and nano-holes<sup>75, 81</sup> can be made by reactive ion etching (RIE) of the polystyrene mask prior to metal deposition. This RIE step is useful to remove material from the surface of the sample by chemical reactions and physical bombardment with gaseous plasma that in turn enhances the versatility of nanosphere lithography. Sometimes this can be used to alter the sizes and the shapes of fabricated nanotriangles and gaps between a nanotriangle pair can also be reduced.<sup>81</sup> Theoretical simulation has predicted that the surface plasmon resonance of such a nanotriangle pair is very strong especially when the gap is smaller than 100 nm.<sup>32</sup> Nui et al. reported another method by which nanohole array can be made by coating the sample surface with polyelectrolyte followed by gold nanoparticles on the samples prepared by nanosphere lithography.<sup>82</sup>

Herein, the technique of NSL is used and adapted with the aim to fabricate substrates for surface enhanced spectroscopy. The gap between the adjacent nanotriangle and the size of the nanotriangle array was varied by changing the diameter of the polystyrene particles used. The samples produced were characterized using scanning electron

microscope (SEM), atomic force microscopy (AFM), optical microscopy and determining the extinction spectra.

## 2.2 Materials and Methods

The fabrication of the substrates is done using nanosphere lithography, in which the glass coverslips are deposited with polystyrene microspheres; it is then followed by gold deposition. Polystyrene microspheres were deposited on a cleaned glass slide by the air-water interface transfer followed by drying the sample, then gold is deposited on top of the thin titanium layer which acts as an adhesion layer, and it is then sonicated in ethanol to obtain the nanotriangle array. Finally, this substrate can be used to enhance the Raman signal or fluorescence depending on the distance of the probe from the gold nanostructures.

### 2.2.1 Reagents

Microscope coverslips ( $22 \times 22 \times 0.15$  mm) were purchased from VWR International, Mississauga, Canada. Acetone was purchased from Sigma- Aldrich. Ethanol (100%) was purchased from Commercial Alcohols, Ontario, Canada. Nochromix was purchased from Godax Laboratories Inc, Maryland, US. Sulfuric acid and ammonium hydroxide were purchased from Caledon Laboratories, Ontario, Canada. Hydrogen peroxide (30%, v/v) was obtained from EMD Inc, Mississauga, Canada. Polystyrene nanospheres (10%, w/w) of various diameters 0.43, 0.65 and 1.00  $\mu\text{m}$  were

purchased from ThermoScientific Co, California, US. Sodium dodecyl sulfate (SDS) was obtained from Sigma-Aldrich, Canada.

### 2.2.2 Cleaning of Glass Slides

Microscope coverslips were sonicated in acetone for 5 min and then cleaned in Nochromix (oxidizing white crystalline solid) dissolved in concentrated sulfuric acid for 15 minutes. This treatment removes the dirt and organic impurities from the glass slides. Then the slides were rinsed in Milli-Q ultrapure ( $18\text{M}\Omega\cdot\text{cm}$ ) water several times. These were sonicated for 1 hour in the mixture of ammonium hydroxide: hydrogen peroxide: ultrapure water ( $18\text{M}\Omega\cdot\text{cm}$ ) in ratio of 5:1:1. This treatment makes the glass surface hydrophilic which is needed for nanosphere lithography. The glass slides were sonicated for 15 minutes in water. These were stored in petri dish filled with water until needed for sample preparation.

### 2.2.3 Preparation of Sample by Nanosphere Lithography

Polystyrene microspheres solution was equilibrated to room temperature before use. Thereafter,  $30\mu\text{L}$  aliquot of microspheres suspension was mixed with  $30\mu\text{L}$  of ethanol (100%). Coverslips were dried and a  $20\mu\text{L}$  mixture of the microspheres in ethanol was transferred on top of the coverslip. This was immediately introduced in the air-water interface of a 6 cm petri dish filled with ultrapure water ( $18\text{M}\Omega\cdot\text{cm}$ ). The coverslip floated on the air-water interface and the solution spread out from the coverslip to the air-water interface. After the dispersion of the solution, the coverslip sank to the bottom of the petri dish. Diffraction pattern was observed on the air-water interface of the petri dish.



A drop of 2% (w/v) sodium dodecyl sulfate solution in water was added to further group the microspheres into an ordered monolayer. The microsphere monolayer was finally picked up using a wet cover slip and was allowed to dry under a petri dish undisturbed overnight. The top view of the sample obtained can be seen in Figure 2-2a.

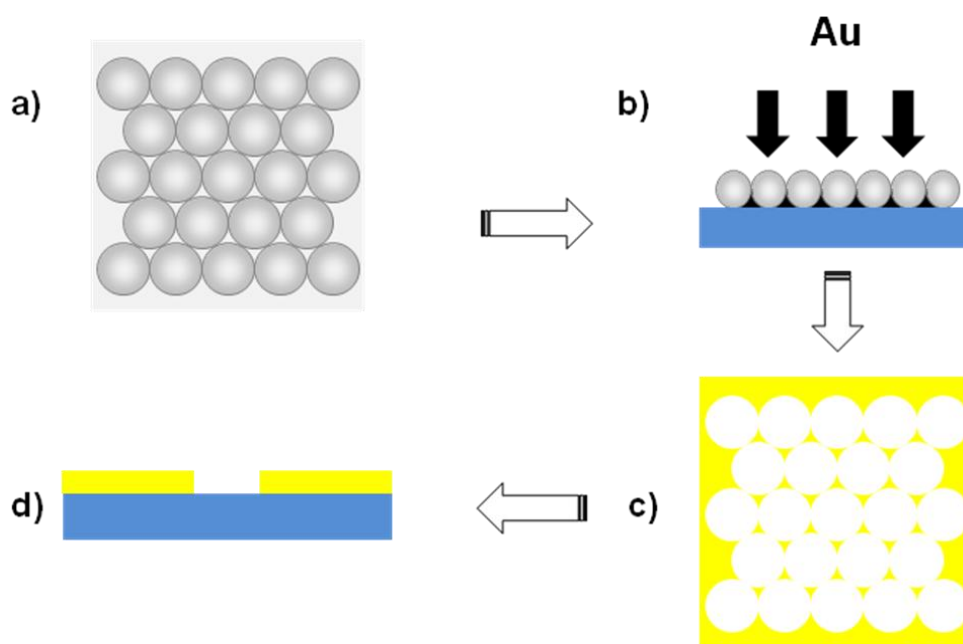


**Figure 2-2** Schematic illustration of sample at various stages: a) top view of polystyrene nanospheres on glass slide, b) deposition of Au, c) top view of nanotriangles after removing polystyrene particles, d) side view of nanotriangles after particle removal

#### 2.2.4 Gold Deposition

The next step is the deposition of gold as shown in Figure 2-2 b. E-beam deposition of materials in a vacuum is one of the best methods to deposit thin metal films with homogenous surface on the NSL masks. Figure 2-3 shows the schematic of the chamber in which the deposition is carried out. The electron beam is used as a heat source. When e-beam collides with the solid surface of the metal, its kinetic energy is consumed in

excitation of secondary emission, X-ray radiation and heating. The kinetic energy of this beam is transformed into thermal energy in the subsurface of the metallic substance which needs to be evaporated. This results in the vapor cloud of metal that condenses on the substrate. The accelerating voltage of 20-25kV is used. This process is carried out in a vacuum  $10^{-4}$ - $10^{-6}$  Torr. <sup>83</sup>

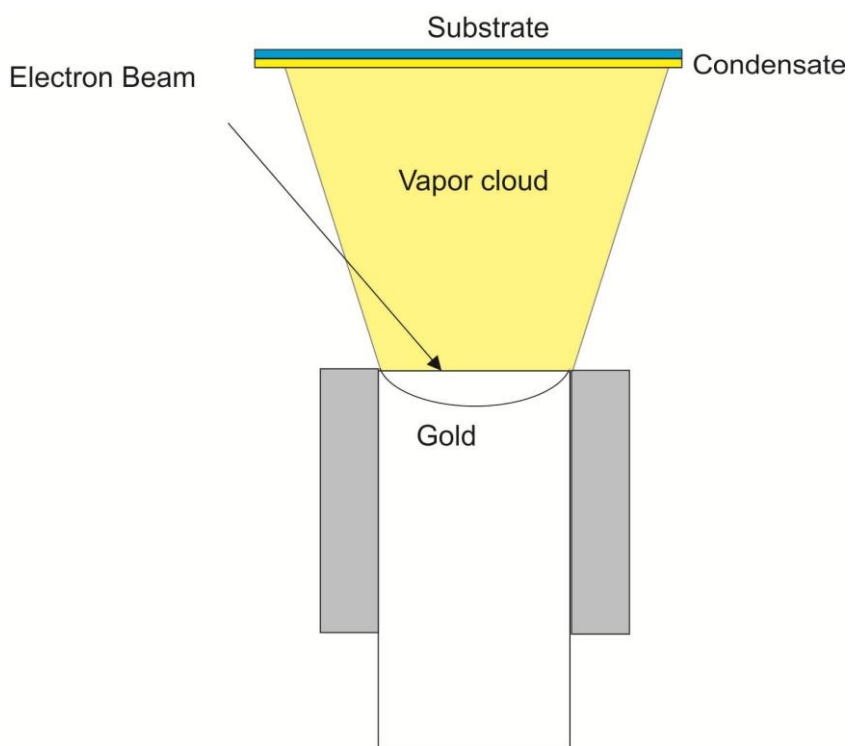


**Figure 2-3** Electron beam evaporation of gold on the sample <sup>83</sup>

After the sample dried, 3 nm of titanium and 30 nm of gold were deposited on the sample using electron beam evaporation (Hoser) in the nanofabrication facility. It took about an hour to deposit the metallic layers on the sample and these metals were deposited at rate of 0.5Å/s.

## 2.2.5 Lift- off

The polystyrene particles were removed by sonicating the sample in ethanol for about a minute. The sample was then dried with nitrogen and it was placed in the sample holder. Figure 2-2 c and d shows the illustration top view and side view after lift-off. After this step the nanotriangles produced can be characterized by various techniques.

## 2.2.6 Surface Characterization of the Samples

### 2.2.6.1 Optical Images

Bright field optical images were obtained using an Olympus IX 71 microscope equipped with a CCD camera.

### 2.2.6.2 Scanning Electron Microscopy (SEM)

The principle of SEM is that the electron beam is focused into a small diameter electron probe which is scanned across the sample surface, making use of the magnetic field that can change the direction of the beam. The electron source used can be a tungsten filament. Above the specimen, there are lenses which act as condenser lenses that are used to focus the beam on the sample. The electron probe of an SEM is scanned horizontally across the sample in two perpendicular directions. The electron beam generated goes through the condenser lenses and then the objective lens and then to the sample where the secondary electrons are deflected towards the detector.

The detector is asymmetrically positioned such that elevated surface areas which face the detector appear bright while the holes and crevices appear darker. Then the signal is amplified and it is sent to a display device like the computer screen. It is

important to make sample conductive, as in the case of insulating samples, surface charges build up and deflect the course of electrons. Hence, non-conductive sample is usually deposited with osmium layer or carbon to make it conductive and prevent surface charging.<sup>84, 85</sup>

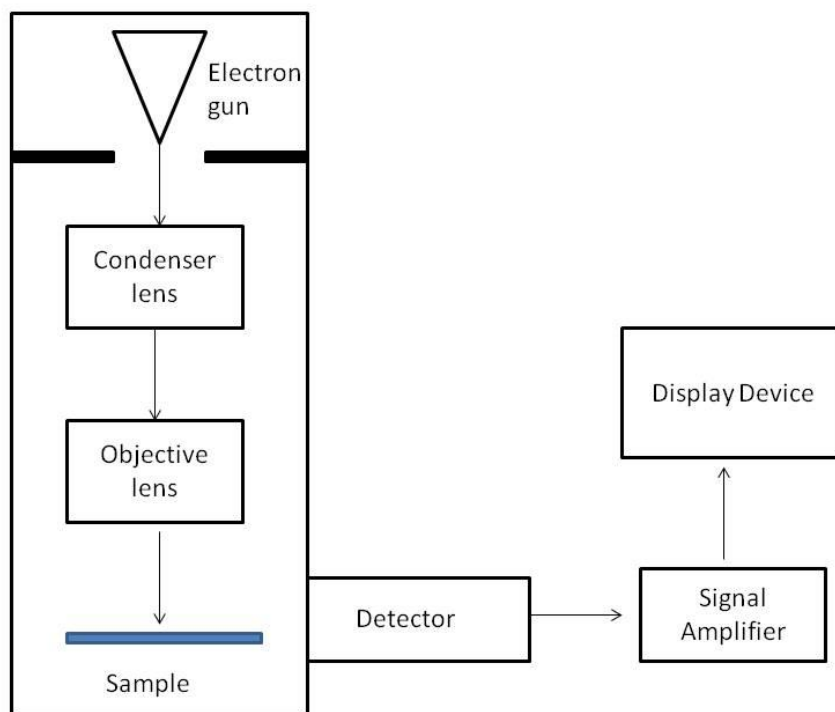


**Figure 2-4** Schematic diagram of a scanning electron microscope with CRT display<sup>85</sup>

SEM images of the samples (0.43, 0.65 and 1.00  $\mu\text{m}$ ) were taken using LEO Zeiss 1530 SEM at the Nanofabrication facility. 3nm of osmium was sputtered, prior to imaging on the samples to make them conductive.

### 2.2.6.3 Atomic Force Microscopy (AFM)

AFM is a powerful scientific instrument that is capable of generating topographical images of the surface of a sample with atomic resolution under best experimental condition. Figure 2-5 represents the setup of an AFM. The most important part of the AFM system is a sharp tip made generally of silicon or silicon nitride, which is mounted to a cantilever; this is scanned across the sample, and the changes in the attractive and repulsive forces between the tip and sample causes a deflection in the cantilever.<sup>86</sup> In the contact mode, the tip operates in the repulsive regime, while in the noncontact mode it operates in the attractive regime. In the tapping mode, the cantilever is made to vibrate at close to its oscillation frequency and the proximity of the surface is determined by damping of this oscillation.<sup>84</sup>

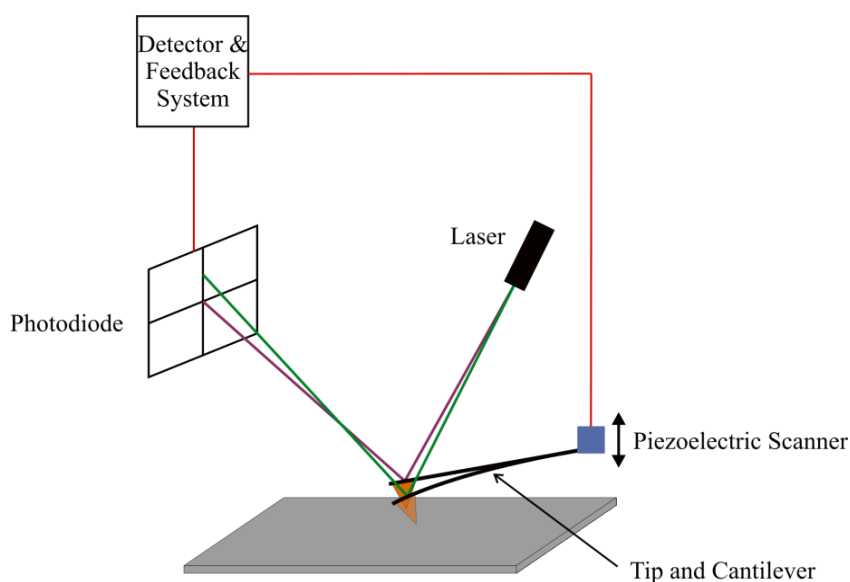


**Figure 2-5** A simplified schematic diagram of the basic setup and main components of the AFM; the laser deflection off the cantilever is directed onto the photodiode after the tip encounters a surface feature<sup>86</sup>

The deflection is monitored by laser beam deflection off the back of the cantilever, which is directed to a quadrant photodiode. As the tip encounters a feature on the surface, the cantilever begins to deflect, and a feedback loop mechanism applies voltage to the piezoelectric scanner that will actuate the tip in the appropriate z-direction to return the cantilever to its deflection set point. The voltage changes are correlated to tip displacement, and can be plotted to reveal the topographical image of the surface of the sample as well as many other parameters characteristic of the sample's surface.<sup>86</sup>

AFM images were collected with the Nanowizard II system (JPK instruments) in tapping mode. A silicon cantilever with a spring constant of 39 N/m (NCL-20, Nanoworld) was used. Images were processed using the JPK Imaging Software and Gwyddion.

#### 2.2.6.4 Extinction Spectrum

Extinction spectrum includes the contribution of the absorption and the scattering of the elastic light. The localized surface plasmon resonance (LSPR) extinction wavelength maximum,  $\lambda_{\max}$ , is primarily sensitive to the dielectric constant of the material,  $\epsilon$ , or the refractive index,  $n$ , as well as the geometry and dimensions of the metallic nanopattern. The value of wavelength maximum can be determined by UV-visible spectroscopy in transmission measurements.

For our patterns, we have utilized a home-made spectrometer to perform measurements on a small surface area in the order of 60 to 100 microns in diameter. This setup consists of a fibre bundle and a set of microscope objectives as shown in Figure 2-

6, the objectives are used to produce a parallel beam with diameter 60-100 microns. After emerging from the sample, the light is collected in transmission by the third microscope objective and its intensity is measured by a CCD after going through the spectrometer. It is important to determine the maximum wavelength as this value should be close to the excitation wavelength used for surface enhanced spectroscopies.<sup>17</sup>

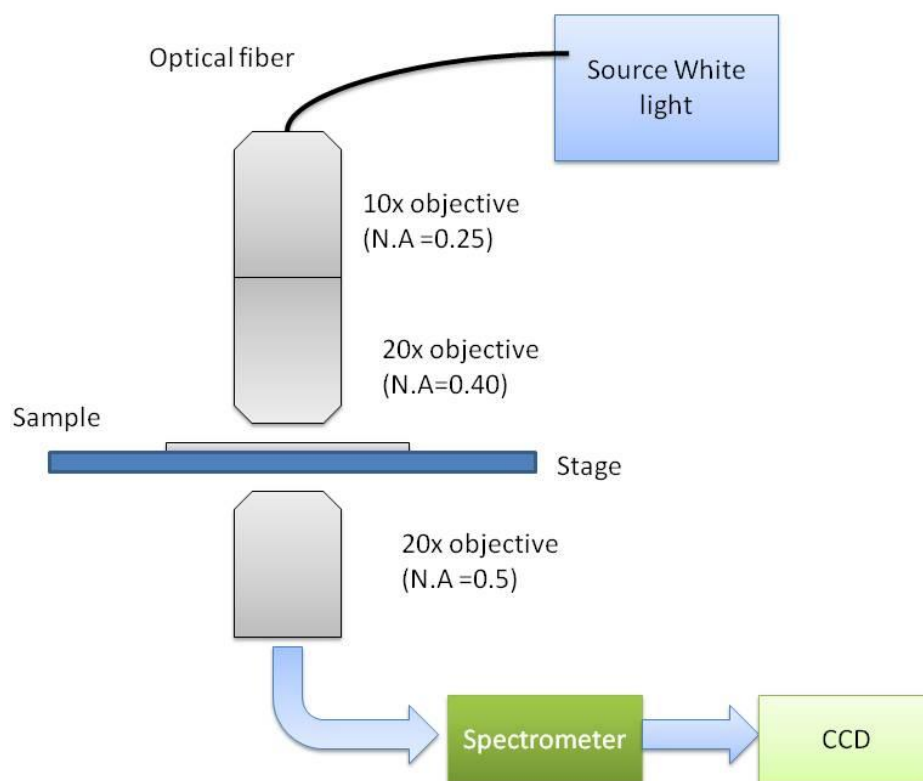


**Figure 2-6** Schematic of the extinction spectra setup

Optical extinction spectra, of the nanopattern prepared by 0.43, 0.65 and 1.00  $\mu\text{m}$ , was obtained using optical microscope in the range of 450-850nm. A white light source (halogen lamp) was connected to a 100  $\mu\text{m}$  optical fibre. At the end of the tip the beam was first expanded using a 10 x, N.A. 0.25 objective and then collimated on the sample

with the 20 x, N.A. 0.40 objective. The transmitted light was collected with a 20 x (N.A. 0.5) objective and sent to the spectrometer for spectral analysis as depicted in the Figure 2-6. The spectra were recorded by using the following acquisition conditions: visible light, pinhole open at 1000 $\mu$ m, 20x (N.A.0.5) objective, 30 accumulations, grating 150 grooves/mm and an integration time of 1s.

## 2.3 Results and Discussion

### 2.3.1 Surface Characterization of the Nanotriangle Array

#### 2.3.1.1 Fabrication of Polystyrene monolayer

The deposition of polystyrene microspheres produced a monolayer on the glass coverslip. Many factors such as dilution of polystyrene solution with ethanol, drying the sample, introducing the mixture into the air-water interface and using MilliQ water instead of deionized water were taken into account to improve the uniformity of the monolayer.

One of the main challenges of the fabrication of the monolayer was the determination of the dilution ratio for polystyrene solution with ethanol. Different dilution ratios were used for polystyrene solution and ethanol such as 1:2, 1:3 and 1:1 but it was found that 1:1 gave the best result. It was seen that if the mixture was too dilute, it failed to form a monolayer on the coverslip. When really concentrated mixture was used, then stacking of the polystyrene spheres on top of each other was observed.



Different methods for drying the sample were also tried such as air drying or drying the samples in control atmosphere over long period of time so that the sample dried slowly. Sometimes the monolayer failed to organize on the air-water interface; instead the mixture of polystyrene settled at the bottom of the petri dish. This issue was resolved by slowly introducing the slide containing the solution into the petri dish. It was noticed that the petri dish containing water needed to have a positive meniscus for formation of the organized monolayer. MilliQ water was needed for the formation of an organized monolayer. It was observed that it was difficult to fabricate single layer nanosphere arrays which cover a large surface area for small nanospheres (0.438  $\mu\text{m}$ ) as reported by Chang et al.<sup>81</sup>

It has been reported that formation of a monolayer is influenced by pH when the polystyrene particles are stabilized by carboxylic acid group or sulfate group.<sup>73</sup> The use of a surfactant also has a noticeable influence on the formation of monolayer. The surfactant molecules accumulate at the air-water interface and form a soft barrier in monolayer formation process, facilitating the packing of particles into a 2D crystal lattice. The detaching colloids are pushed against the surfactant layer; as a result this pushes the particles together, facilitating the formation of 2D crystalline monolayer. The monolayers which were floating in the presence of surfactants exhibit higher mechanical stability and fracture less easily at the edges.<sup>73</sup>

Therefore, under the optimum conditions described, an organized monolayer of polystyrene microspheres over a glass coverslip was obtained. As this monolayer is a naturally occurring 2D crystal, it shows a variety of defects like nanosphere polydispersity, site randomness, point defects and line defects. Figure 2-7 are the optical

images of the sample taken when particles were deposited on the glass slide followed by gold deposition and then lift-off. Typical defect free domain sizes are in the 10-100  $\mu\text{m}^2$  range.<sup>13</sup>

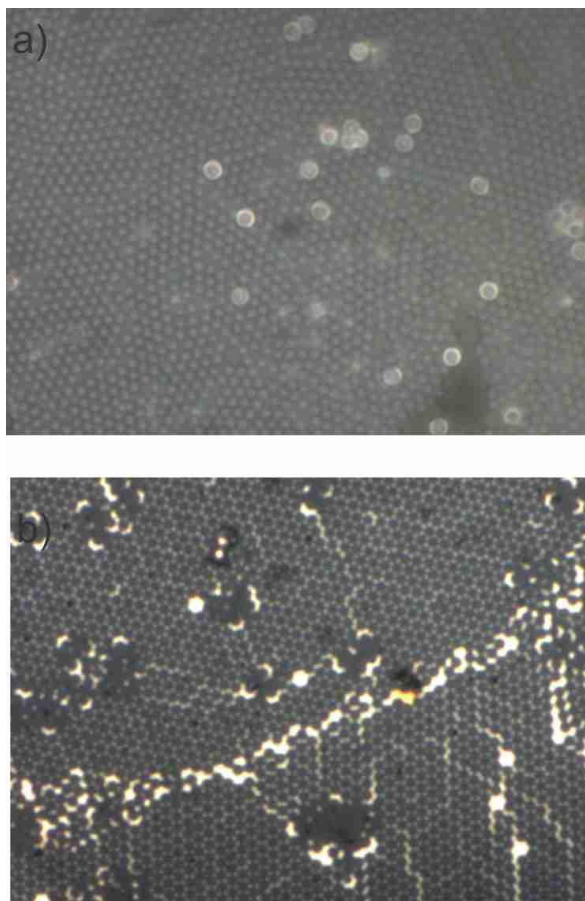


**Figure 2-7** Optical images objective 100x (N.A. 0.95) a) sample with polystyrene particles, 1.00  $\mu\text{m}$ , b) same sample after gold deposition and lift -off of particles

### 2.3.1.2 Uniformity of the Array

The uniformity of the polystyrene monolayer is determined by observing the sample optically and under the SEM. The samples were prepared with different sizes of polystyrene nanospheres (0.43, 0.65 and 1.00  $\mu\text{m}$ ), before and after removal of particles,

are shown in Figure 2-8 using scanning electron microscope (SEM). Table 2-1 approximately gives the value of the height (perpendicular bisector) of nanotriangle and distance between two adjacent nanotriangles. However, the distribution over the gaps can be larger than 50% depending on the sample preparation procedure. While observing the sample in the SEM, some unexpected variations were discovered that can be seen in Figure 2-8. The polystyrene microspheres solution consisted of alternate size spheres which has affected the fisher pattern.

**Table 2-1** Height and the distance between nanotriangles given in each case

<b>Particle Size</b>	<b>Height of Nanotriangle</b>	<b>Distance between nanotriangles</b>
<b>0.43 <math>\mu\text{m}</math></b>	110-120 nm	0.13-0.14 $\mu\text{m}$
<b>0.65 <math>\mu\text{m}</math></b>	190-200 nm	0.15-0.16 $\mu\text{m}$
<b>1.00 <math>\mu\text{m}</math></b>	250-260 nm	0.18-0.19 $\mu\text{m}$

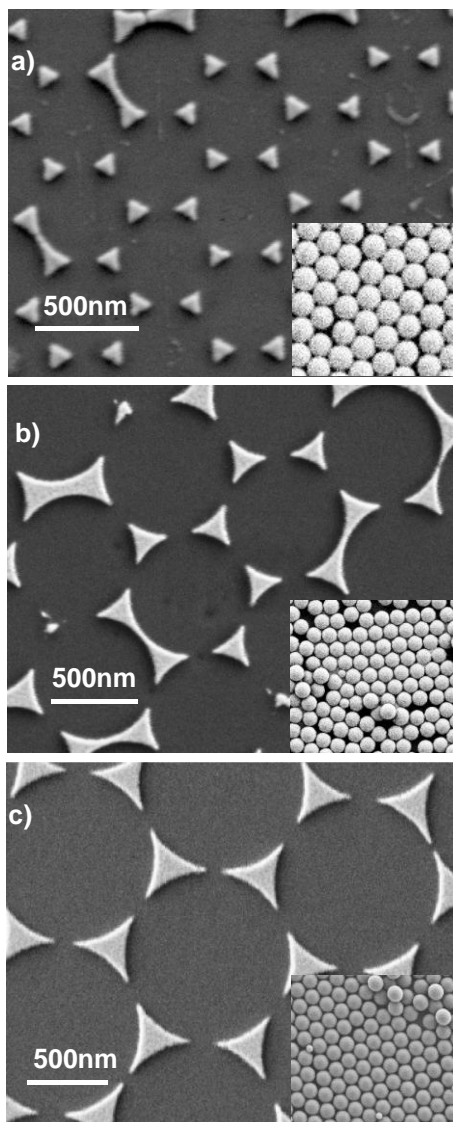


**Figure 2-8** SEM images of a) 0.43  $\mu\text{m}$  b) 0.65  $\mu\text{m}$  c) 1.00  $\mu\text{m}$  gold nanotriangle arrays and monolayer of polystyrene nanospheres showed in right bottom corners

### 2.3.1.3 Thickness of gold deposited

The topography of the nanotriangles was explored by tapping mode AFM. Several pieces of information can be extrapolated from these images, the first being the thickness of gold and titanium which corresponds to 33nm. Similarly, the image also confirms that the lift-off of polystyrene particles after the gold deposition was successful and efficient.

The gap between the nanotriangles and the height of the nanotriangles can be compared with the SEM measurements. It was found when compared with AFM measurements that the values obtained were accurate from the SEM measurements. Figure 2-9 shows the AFM images obtained for sample prepared by  $0.438\ \mu\text{m}$  polystyrene nanospheres.

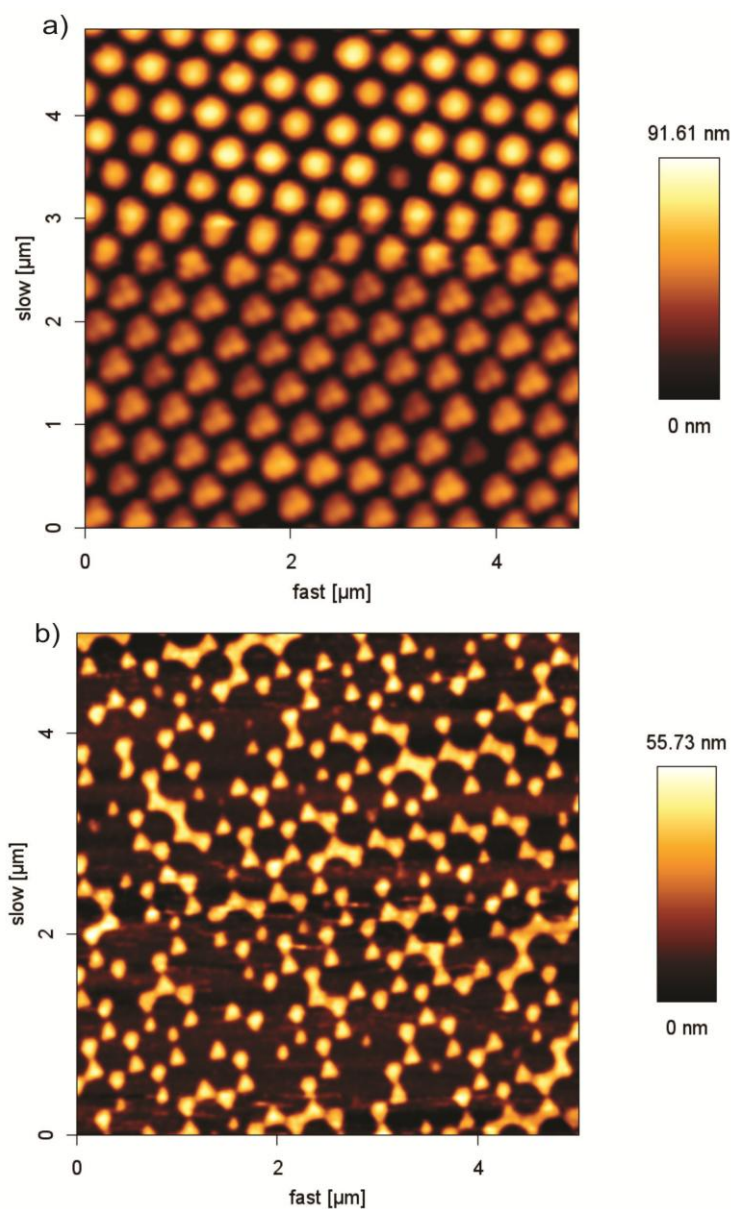


**Figure 2-9** AFM image ( $5 \times 5\ \mu\text{m}$ ) a) polystyrene particles coated with gold ( $0.43\ \mu\text{m}$ ), b) nanotriangles array after the lift-off

#### 2.3.1.4 LSPR wavelength of nanotriangle arrays

The optical signature of a metallic nanoparticle is the localized surface plasmon resonance (LSPR). This resonance occurs when the correct wavelength of light impinges on the ensemble of nanoparticles, causing the plasma of conduction electrons to oscillate collectively. The term LSPR is used because this collective oscillation is localized within the near surface region of the nanoparticle. The two consequences of exciting the LSPR are: selective photon absorption and generation of locally enhanced or amplified electromagnetic fields at the contour of the individual or interacting ensembles of nanoparticles.<sup>13, 87</sup>

Experimentally, as the shape or size of the nanoparticle change, the surface geometry varies causing a shift in the electric field density on the surface. This causes a change in the oscillation frequency of the electrons, generating different cross sections for optical properties including absorption and scattering. Changing the dielectric constant of the surrounding material has an effect on the oscillation frequency due to varying ability of the surface to accommodate electron charge density from nanoparticles.<sup>46</sup>

NSL can be particularly useful because both the large and small nanotriangles can be made with this technique.<sup>13</sup> This technique is limited in the absorption intensity due to the presence of only a monolayer of nanoparticles. However, prismatic particles have sharp corners; the absorption enhancement is good that only ten thousand particles give excellent absorption.<sup>88</sup> The plasmon resonance absorption has an absorption coefficient orders of magnitude larger than strongly absorbing dyes.<sup>46</sup> The frequency and intensity of a plasmon resonance are determined primarily by the intrinsic dielectric property of a given metal; the dielectric constant of the medium in contact with the metal and the

pattern of surface polarization. As such, any variation in the shape or size of a metal particle can alter the surface polarization changes the plasmon resonance, leading to increased detection sensitivity.<sup>29, 46</sup>

As stated earlier, in order to get efficient enhancement from the sample, it is necessary that the plasmon wavelength of the platform matches the wavelength of the incidence laser. The LSPR frequency was determined from the extinction spectrum measured for each substrate and is reported in Figure 2-10 in the 400-850nm spectral range. The LSPR wavelength for 0.43  $\mu\text{m}$  substrate was determined to be in the range of  $600 \pm 15\text{nm}$  while for the 0.65 $\mu\text{m}$  sample it was between  $650 \pm 15\text{nm}$  and the sample prepared by 1.00  $\mu\text{m}$  had the range of  $450 \pm 15\text{nm}$  and  $770 \pm 15\text{nm}$ . Figure 2-10 shows the extinction spectra of all the three samples. The dipole resonance arises from one side of the sphere surface being positively charged, whereas the opposite side is negatively charged, giving the particle itself a dipole moment which reverses sign at the same frequency as the incident light. The weak quadrupole resonance arises from energy losses that cause non-uniformity of the incident light across the sphere and the formation of two parallel dipoles of opposite signs.<sup>29</sup>

The nanotriangle facilitates increased charge separation when polarized along one of the edges and thus the spectra exhibit peaks shifted towards longer wavelengths.<sup>15</sup> The results obtained prove that the plasmon resonance can be tuned across the visible region by changing the aspect ratio by changing the different diameter of polystyrene nanospheres.

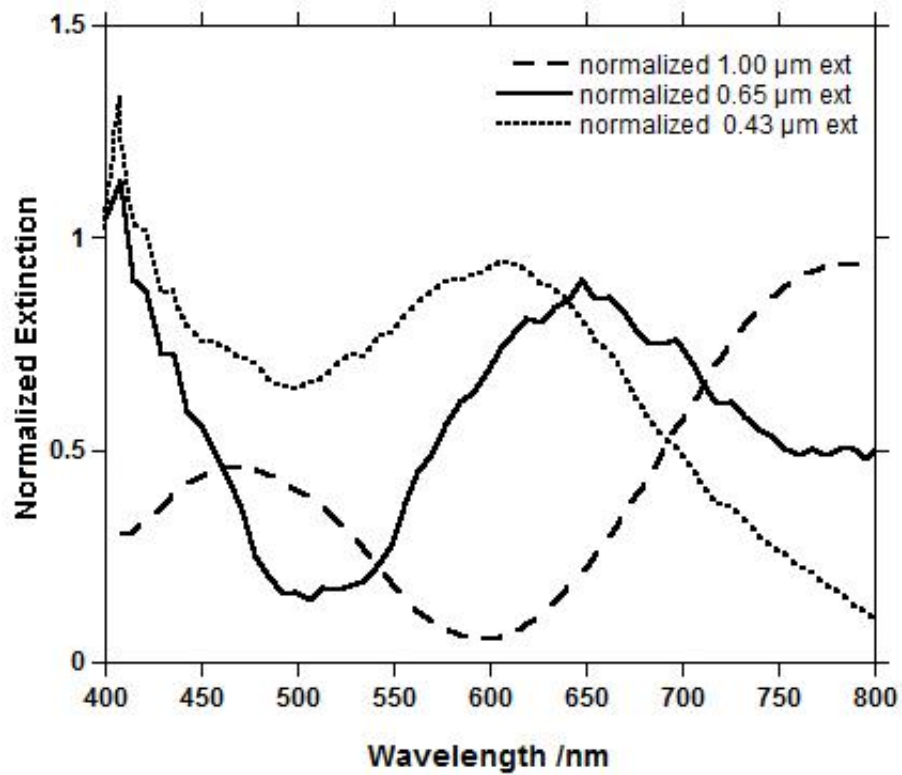


**Figure 2-10** Typical extinction spectra of 0.43, 0.65 and 1.00 μm nanotriangle sample



## 2.4 Conclusion

Nanostructures have been made using many different microfabrication techniques to study various specimens for spectroscopic enhancement. In this thesis, a simple method to make nanotriangles have been used by the combination of nanosphere lithography, followed by gold deposition and lift off to form large area ( $>100\mu\text{m}^2$ ). The size of the nanotriangles can be tailored by changing the particle size of the polystyrene microspheres. These samples were characterized by optical microscopy, scanning electron microscopy, atomic force microscopy and by determination of extinction spectra of sample. It is proved that this can be used to make nanotriangle arrays which can be used to probe the molecule of interest.

## Chapter 3

### 3 Surface Enhanced Raman Spectroscopy

This chapter begins with the description of surface enhanced Raman spectroscopy and its recent applications are discussed. Following this, the materials and methods needed to functionalize the sample is explained. Finally, the Raman spectra of benzenethiol and azobenzene thiol are examined.

#### 3.1 Introduction

Raman spectroscopy is an important and powerful technique for determining the molecular structure of substances. The Raman signal is enhanced by several orders of magnitude for molecules adsorbed onto the roughened surfaces or nanoparticles of silver or gold metal.<sup>89-92</sup> After more than forty years of development,<sup>6</sup> surface enhanced Raman spectroscopy (SERS) has been proved to be a versatile and sensitive analytical technique as it allows measurement of Raman spectra for concentration of solution in micromolar range.<sup>93</sup>

This technique has been used to detect biomolecules such as DNA<sup>94, 95</sup> and amino acid,<sup>96</sup> pollutants in the environment like polycyclic aromatic hydrocarbon,<sup>97</sup> explosives in trace amount<sup>55</sup> and to study important biological processes like the enzymatic activity in a single cell.<sup>98</sup> Efforts have also been made for single molecule detection of molecules employing SERS.<sup>90, 99</sup>

The origin of surface enhanced Raman scattering can be attributed to two mechanisms: the electromagnetic mechanism, which is based on surface plasmon

resonance with a factor of  $10^6$ - $10^8$  enhancement, and the chemical mechanism, which is based on charge transfer between the molecule and the substrate with a factor of  $10$ - $10^2$  enhancement. It has been reported that the molecules caught in the junction between nanoparticles have larger SERS signal enhancement as the coincident local electric fields furnishes “hot-spots” for SERS, thus the substrate should possess a huge surface area in order to absorb more target molecules.<sup>100, 101</sup>

The selection rules for SERS are different compared to conventional Raman spectroscopy because the strength of the local electromagnetic field at surface has its maximum in the direction normal to the surface, vibrational modes arising from the changes in polarizability along with a change of the normal coordinates of the adsorbate which are perpendicular to the surface will be preferentially enhanced. Since the enhancement effect strongly depends on the physical properties of the substrate, different kind of substrate have evolved.<sup>2</sup> Most common nanostructures reported for SERS are Au nanoparticle arrays,<sup>87</sup> multi bow-tie structures,<sup>102</sup> gold nanorods,<sup>103</sup> silver islands,<sup>104</sup> nanocubes,<sup>100</sup> nanocages<sup>105</sup> and gold moon crescent.<sup>106</sup>

SERS substrates such as nanoparticles with sharp edges or corners as well as sharp tips are of significant interest in this field.<sup>100</sup> Local electric field enhancements are seen for all types of noble metal nanoparticles, but even greater local field enhancements are observed at sharp surface features such as corners of gold nanocubes,<sup>100, 107</sup> where the curvature radius is smaller than the size of the nanoparticle. This phenomenon is known as the “lightning rod” effect on surface enhancement.<sup>100, 107, 108</sup>

A self-assembled monolayer (SAM) provides several advantages with respect to sensitivity and quantification. The high sensitivity arises from maximum coverage with the molecule of interest. Molecules within a SAM are uniformly oriented with respect to the surface normal. This leads to a reproducible SERS signature with only a few dominant Raman bands, which is beneficial for quantification. SAM also has a protective feature as it minimizes the co-adsorption of other molecules onto the surface of the SERS substrates, hence reducing the spectral interferences caused by other molecules.<sup>21</sup>

Encapsulation can completely eliminate this issue by avoiding desorption of the molecule of interest from the metal surface and adsorption of other molecules from the environment the surface. Different encapsulation materials have been reported such as silica,<sup>109</sup> organic polymers<sup>110</sup> and biopolymers.<sup>111,21</sup>

One of the biggest challenges facing SERS on colloidal nanoparticle substrates is reproducibility of the nanoparticles. It is important to know both the number of nanoparticles in solution and the number of molecules sampled during the experiment for the quantification of analyte and calculation of SERS enhancement factors. This can be difficult for colloidal nanoparticles because the number of molecules in nanoparticle junction, which could contribute to the majority of signal, is usually unknown. SERS measurement on self-assembled monolayer (SAM) of the target analyte on the planar gold substrate allow the SAM to be deposited on a smooth gold surface and so the number of molecules sampled can be estimated, but the signals obtained from planar substrate is weaker than the signal obtained for a colloidal nanoparticle and it also requires a long acquisition time.<sup>112</sup>

Recently, a new technique was developed i.e. tip enhanced Raman spectroscopy (TERS), as the name suggests, it enhances the Raman signal of the molecule of interest along with the spatial resolution. The TERS setup consists of atomic force microscope (AFM) coupled with a Raman spectrometer. TERS signal is generated by sample molecule present within the optical near field of a strongly confined and enhanced electromagnetic field at the apex of the metallic or metal-coated tip which is excited by focused laser beam. Most often silver or gold is employed as enhancing metal, and the tip-sample distance is in the range of 10 nm.<sup>113</sup> The total Raman scattering signal from the tip is rather weak, so TERS studies have been limited to molecules with large Raman cross sections such as dyes<sup>114</sup> and carbon nanotubes.<sup>115</sup> The major drawback of this technique is the temperature rise beneath the tip apex upon irradiation which could affect the sample integrity. The current instrument complexity as well as reproducibility is still very demanding for this technique.<sup>116</sup>

Recently, Tian et al. reported a new approach in which the gold nanoparticles are coated with an ultrathin shell of silica or alumina<sup>92</sup> and have used it to study the Raman spectra of yeast cells and hydrogen adsorption on a crystal surface. The principle behind this approach is that a silica coated gold nanoparticle acts as a gold tip in the TERS system and as a result this technique brings thousands of TERS tips to the substrate surface to be probed. The use of a chemically inert shell coating around the gold nanoparticle protects the SERS active gold nanostructure from contact with the molecule of interest. This technique is known as shell-isolated nanoparticle enhanced Raman spectroscopy (SHINERS).<sup>92, 117</sup>

Herein, the substrates are fabricated using NSL followed by gold deposition and are functionalized with molecules of interest such as benzenethiol and azobenzene thiol. The Raman spectrum for both molecules is recorded with short acquisition time and low laser intensity. The assignment of the vibrational modes of the molecules was done by looking at the values from the literature.

## 3.2 Materials and Methods

### 3.2.1 Reagents

Microscope coverslips (22 ×22 ×0.15 mm) were purchased from VWR International, Mississauga, Canada. Acetone was purchased from Sigma- Aldrich, Canada. Ethanol (100%) was purchased from Commercial Alcohols, Ontario, Canada. Nochromix was purchased from Godax Laboratories Inc, Maryland, US. Sulfuric acid and ammonium hydroxide were purchased from Caledon Laboratories, Ontario, Canada. Hydrogen peroxide (30%, v/v) was obtained from EMD Inc, Mississauga, Canada. Polystyrene nanospheres (10%, w/w) of various diameters 0.43, 0.65 and 1.00 μm were purchased from ThermoScientific Co, California, US. Sodium dodecyl sulfate (SDS) was obtained from Sigma-Aldrich, Canada. Benzenethiol (97%, v/v) was purchased from Sigma – Aldrich, Canada. Azobenzene thiol 2-[4-(4-Decylcycloxyphenylazo)-phenyl] ethyl thiol was prepared in the laboratory by the method reported elsewhere.<sup>25</sup>

### 3.2.2 Fabrication of Nanotriangles

The fabrication of the nanotriangle arrays was performed similar to the procedure outlined in chapter 2, Sections 2.2.2-2.2.5. Briefly, glass coverslips were thoroughly cleaned followed by deposition of polystyrene nanospheres by air- water interface. This sample was allowed to dry overnight and then 3nm of titanium and 30nm of gold was deposited. The polystyrene mask was lifted- off by sonicating the sample in ethanol, making the nanotriangle array.

### 3.2.3 Functionalization of the SERS Platforms

The SERS substrates (0.43, 0.65 and 1.00  $\mu\text{m}$ ) were functionalized with benzenethiol molecule by immersing the samples in a  $10^{-3}$  M solution of this molecule in ethanol for 12 hours. This was followed by subsequent washing of the sample with ethanol to remove excess of benzenethiol. The SERS substrates (0.43, 0.65 and 1.00  $\mu\text{m}$ ) were functionalized with azobenzene thiol molecules. Samples were immersed in a  $10^{-4}$  M solution of the azobenzene molecule in chloroform for 12 hours. This was followed by subsequent washing of the sample with chloroform to remove excess of azobenzene molecules and aggregates non-covalently adsorbed on the gold nanostructure. The Raman spectrum for each sample was then recorded.

### 3.2.4 Raman Spectroscopy

Although Raman effect was already discovered in 1928 by Chandrasekara Raman, the Raman spectroscopic experiments were not carried out until the development of lasers in 1960s. The instrument consists of following parts: an excitation light source, optical microscope, a spectrometer, a detector and a data acquisition unit.

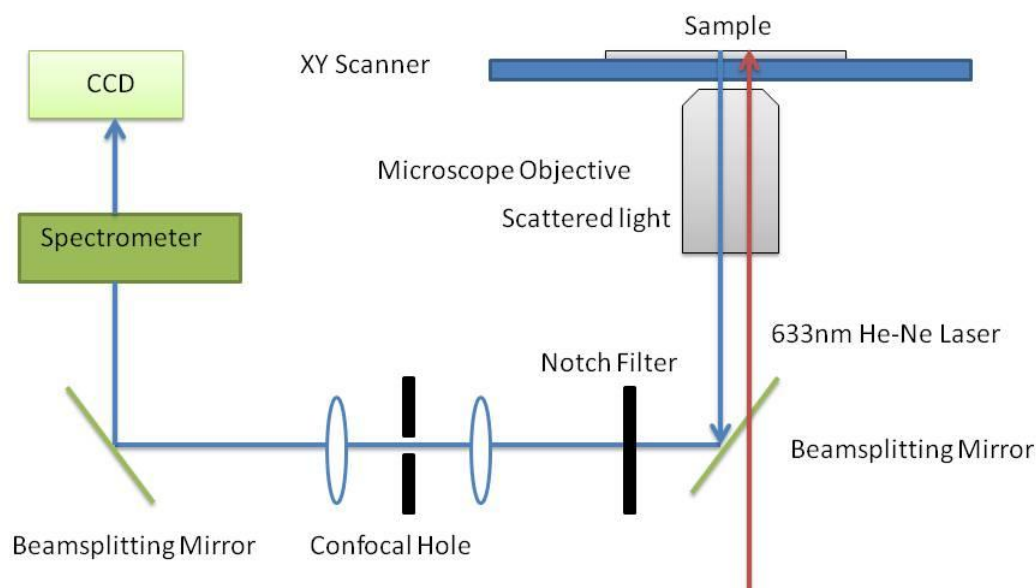


**Figure 3-1** Schematic of confocal Raman spectrometer showing the main components

The excitation light source is always a laser that has a very stable intensity. The Raman signal is proportional to the excitation power but the laser power should be well below the point where the absorption leads to thermal decomposition of the sample. To obtain the highest possible efficiency in combination with the best spatial resolution, an objective with the high numerical aperture should be used. The optical microscope is used to focus the laser light on the sample, to collect the backscattered light and send it to the spectrometer. Moving microscope stages (with a micron and submicron step size) are widely used to conduct Raman mapping experiments. Confocal optical microscope is used to enhance the spatial resolution.

The spectrometer has a twofold purpose: to separate the Rayleigh scattered light from the Raman signal and this done by the notch filter and it also analyzes the collected



optical signal. The spectrometer consists of gratings and mirrors which disperse the signal onto the CCD detector by deflecting each wavelength at a slightly different angle. The number of grooves per millimeter determines the dispersion characteristics. The detector can be a single channel detector (photomultiplier tube, PMT) or multichannel detector (charged coupled device, CCD). PMT has higher sensitivity as compared to CCD but the only disadvantage is that is long acquisition time. CCD records a wide range of wavelengths at the same time. The data acquisition unit is simply a PC interfaced with the detector to store, display and manipulate the data for better data presentation.<sup>24, 118</sup>

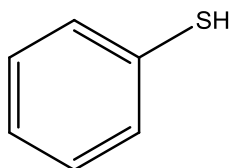
The Raman spectrum of samples functionalized with benzenethiol was recorded on the Raman spectrometer (Horiba Jobin Yvon) using 632.8nm He-Ne laser radiation that is linearly polarized, a confocal pinhole of 100 $\mu$ m, 100x (N.A.0.95) microscope objective, a grating of 600grooves/mm and an integration time of 100s. The spectrum was recorded in the range of 200-1800 $\text{cm}^{-1}$ . The Raman spectrum of the samples functionalized with azobenzene thiol was recorded using a 632.8nm He-Ne laser radiation that is linearly polarized, a confocal pinhole 150 $\mu$ m, 100 x (N.A.0.95) microscope objective, a grating of 600grooves/mm and an integration time of 40s.

### 3.3 Results and Discussion

#### 3.3.1 Assignment of Raman Spectra of Benzenethiol

To determine the efficiency of the SERS platforms, the nanotriangle samples were functionalized with benzenethiol (BT) and the Raman spectra of benzenethiol was

obtained as shown in Figure 3-3 and the vibrational modes observed were compared with the ones reported in literature.<sup>119</sup> It is important to note that the signal of molecule on plain gold was not detected. The assignments of the vibrational modes for BT grafted on the gold surface are summarized in Table 3-1.



Benzenethiol

**Figure 3-2** Structure of benzenethiol (BT)

The following observations are worth mentioning. The S-H stretching ( $2566\text{ cm}^{-1}$ ) and the S-H bending ( $917\text{ cm}^{-1}$ ) in the SERS spectrum are not present indicating the adsorption of benzenethiol onto the gold nanostructure by rupturing S-H bond. The formation of the sharp peak at  $1470\text{ cm}^{-1}$  indicates the formation of Au-S bond formation. The C-S stretching and in plane deformation shows a major change from normal Raman to SERS, it is downshifted by  $20\text{ cm}^{-1}$  in SERS. This shift was probably observed as this mode was involved the movement of the S when the S-H bond broke. The C-C stretching also showed a downshift from  $1572$  to  $1580\text{ cm}^{-1}$  in the SERS.<sup>119</sup> Shifts in peak position are commonly observed in SERS and these arise from differences in chemical environment experienced by the bound and neat species. The differences in relative SERS and normal Raman peak intensities can be attributed to preferential enhancement of the vibration modes oriented perpendicular to the surface.<sup>120</sup> It has been reported through FDTD calculation that the nanotriangle array interacts differently with the incoming beam, depending on its orientation with respect to the input polarization of the

incident light. It was observed that strongest enhancement would be obtained when the sample is irradiated with polarization direction parallel to the bow-tie axis.<sup>121</sup>

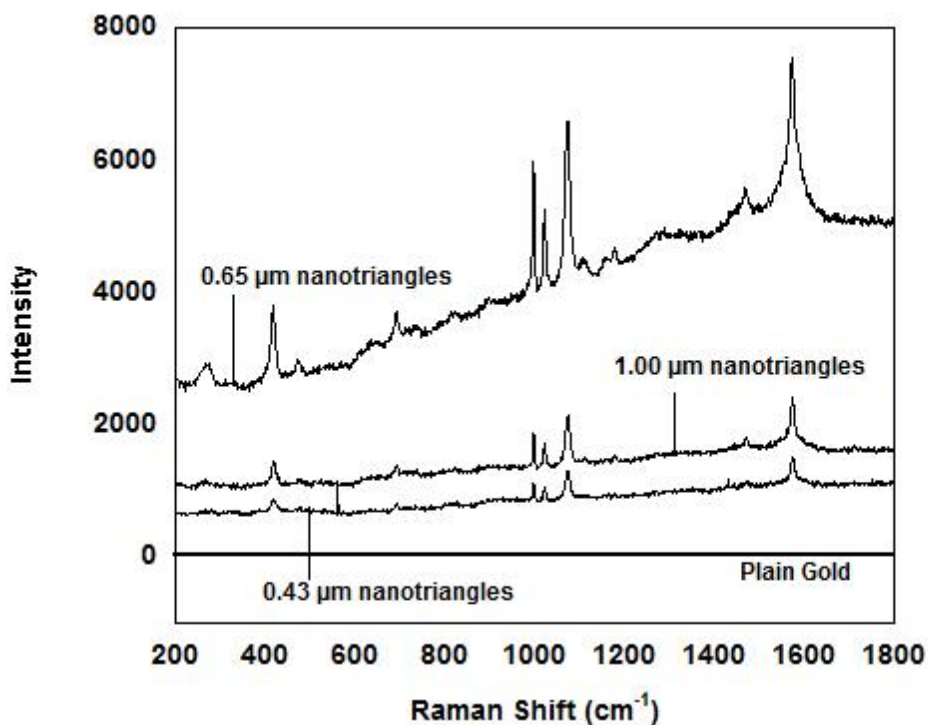


**Figure 3-3** Raman spectra of benzenethiol on nanotriangle sample

**Table 3-1** Assignment of vibrational modes for benzenethiol<sup>119</sup>

Assignment	Shift	Assignment	Shift
Au-S	1470	S-in plane ring def	998
C-S stretching	417-419	In plane ring def	1021
C-H out of plane def	693	C-S stretching +in plane def	1072
C-C-C def	736	C-C stretching	1572

### 3.3.2 Assignment of Raman spectra of azobenzene thiol

The nanotriangle samples were functionalized with azobenzene 2-[4-(4-Decyloxyphenylazo)-phenyl] ethyl thiol (Figure 3-4) and Raman spectra were recorded that are shown in Figure 3-5. The spectra obtained were compared to the spectra of azobenzene reported in literature. Assignment of the vibrational modes is given in Table 3-2. The absence of the peak at  $2590\text{ cm}^{-1}$  indicates the cleavage of the H-S bond and the formation of the self assembled monolayer of azobenzene monolayer on the nanostructured gold surface.<sup>25</sup>

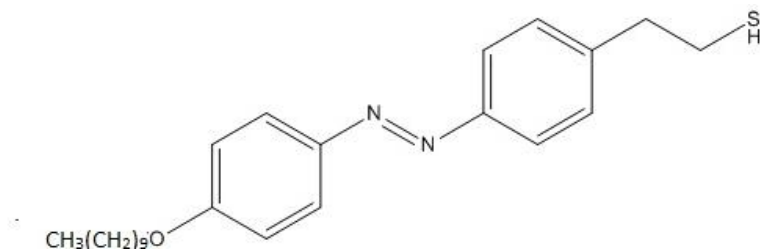


**Figure 3-4** Structure of azobenzene thiol

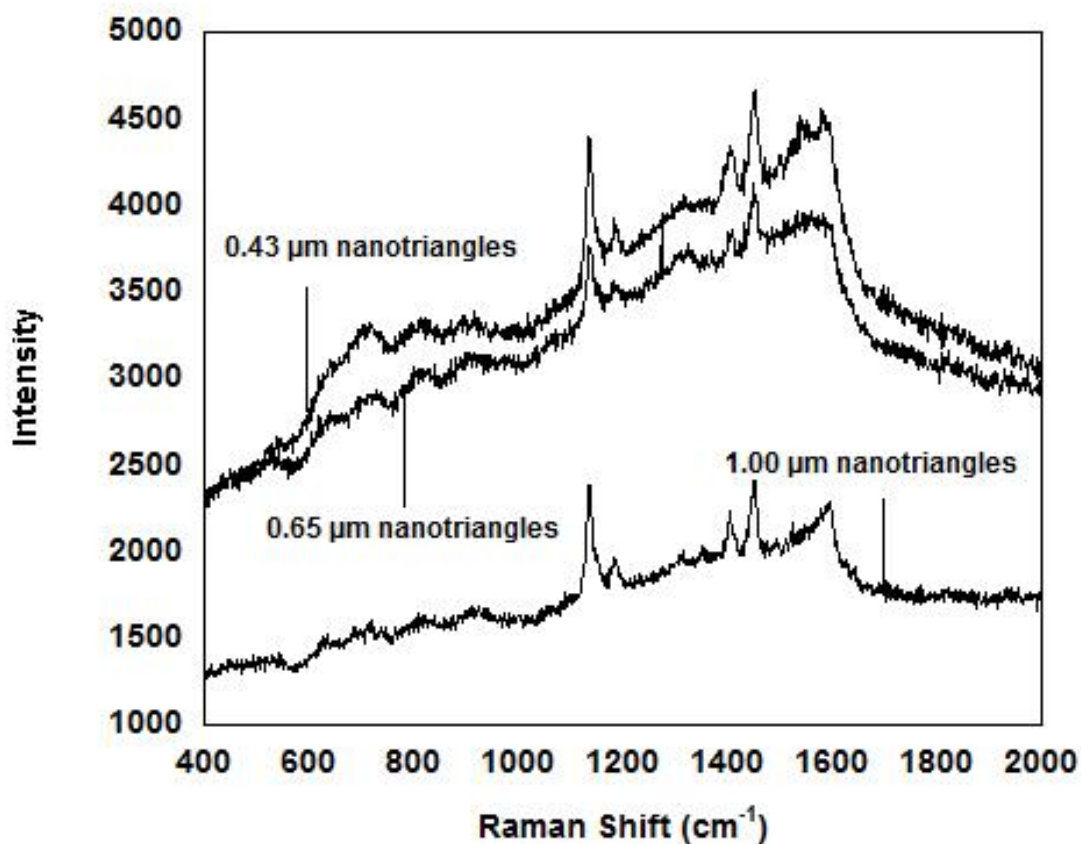


**Figure 3-5** Raman spectra of azobenzene thiol on nanotriangle sample

**Table 3-2** Assignment of vibrational modes for azobenzene thiol molecule<sup>25</sup>

Assignment	Shift	Assignment	Shift
C-H bending	1136	N=N vibration	1400
C-H in plane bending	1183	C=C+CH bending	1452
Ring- N asymmetric	1305	C=C vibration	1602

An azobenzene moiety is known to undergo photoisomerization upon irradiation. When azobenzene molecules are irradiated with a linearly polarized light, if the wavelength matches the absorption of the azobenzene moiety, a trans-cis-trans isomerization is observed and the degree of stability of the cis- isomer depends mainly on the substituents on the azo core unit and vary between 10 hours to millisecond range in solution.<sup>122, 123</sup> However, in our experiments, the use of the excitation wavelength, 632.8 nm, doesn't induce photoisomerization of azobenzene as it is located outside the absorption band of chromophores.

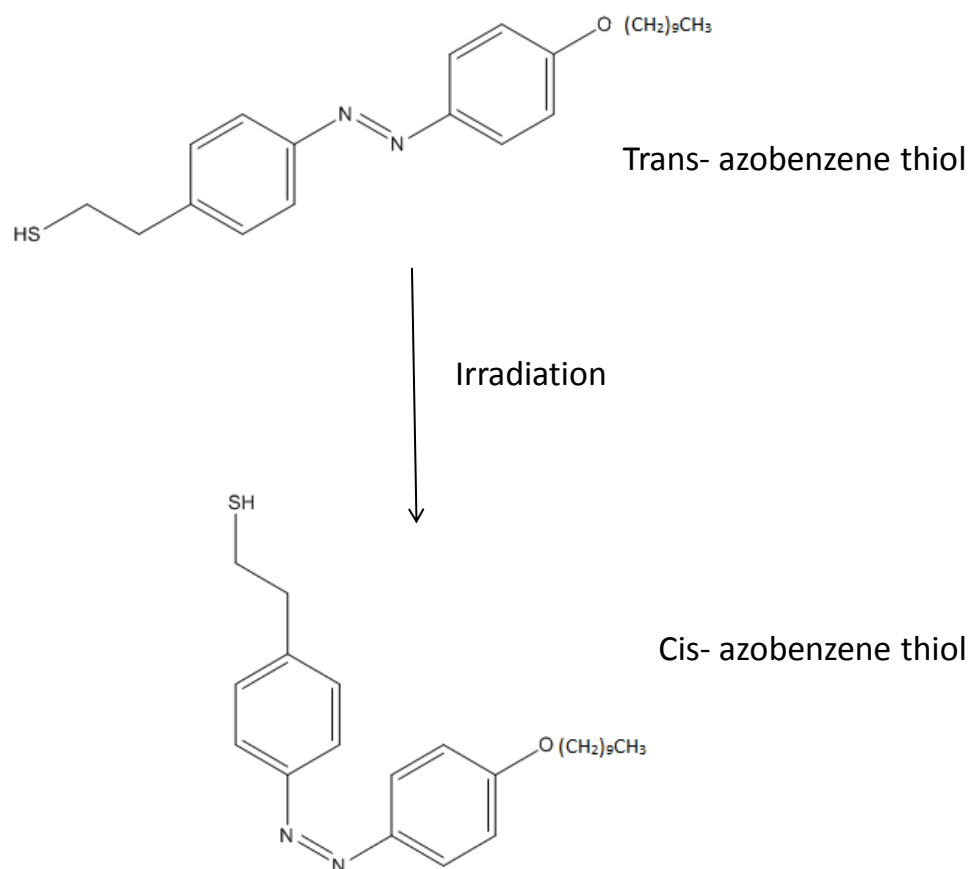


**Figure 3-6** Photoisomerization reaction of azobenzene thiol molecule when irradiated

### 3.3.3 Effect of different size of nanotriangles on the Raman signal

The main advantage of our SERS substrate is that there is no linker molecule or capping molecules are present which might influence the SERS spectra of the molecule of interest. Clean substrate surface is required for the effective adsorption of analyte to the gold surface. The preparation of our SERS substrate is fast and easy as compared to the other preparation methods.

The enhancement of the Raman signal is dependent upon the geometry, size and nature of the metallic substrate but it also depends on the matching of the electric field of both the excitation source and the Raman signal with the plasmon band. To find out that which substrate worked efficiently at 632.8 nm excitation source the enhancement in each case was considered. All the Raman spectra were recorded under same conditions and thus the enhancement can be compared.

In the case of SERS spectra of benzenethiol, the intensity of C-C stretching peak, for 0.65 $\mu\text{m}$  it is 7500 a.u while for 1.00  $\mu\text{m}$  it is 1400 a.u and for 0.43  $\mu\text{m}$  it is 1100 a.u. It is observed that the background for sample prepared by 0.65  $\mu\text{m}$ , is high but the peaks obtained in this case are clear and distinct as compared to the other samples used . All the vibrational modes reported in the literature are intense for the sample prepared with 0.65  $\mu\text{m}$  and 1.00 $\mu\text{m}$  but all of the vibrational modes are less intense in the case of 0.43  $\mu\text{m}$ . In the case of azobenzene, high intensity signal was obtained for 0.65  $\mu\text{m}$  followed by 1.00  $\mu\text{m}$ .

### 3.4 Conclusion

In summary, it is demonstrated that nanotriangle arrays can be fabricated by NSL followed by gold deposition for surface-enhanced Raman spectroscopy (SERS). SERS signal can be tuned by changing the diameter of polystyrene nanospheres used to prepare the samples, which is related to the matching LSPR of the sample with the excitation laser. The SERS platforms were tested against benzenethiol and azobenzene self-assembled monolayers over the gold nanostructures. The assignments of the vibrational modes of the molecules were in accordance with values reported in literature. It is noteworthy that absolutely no enhancement of signal was observed on plain (non-structured) gold.



## Chapter 4

### 4 Mapping hot-spots on nanotriangle array using fluorescence microscopy

This chapter begins with a description of fluorescence enhancement and different research work reported in this field so far. The chapter proceeds to describe the use of nanotriangle array, prepared by nanosphere lithography, for fluorescence enhancement after silica deposition. This results in the generation of individual hot-spots upon the addition of Iris- 5 dye solution. The characterization of the samples prepared is also discussed.

#### 4.1 Introduction

Although discovered almost four decades ago,<sup>6, 124</sup> surface enhancement from a metallic surface has led to renewed interest in spectroscopy up to the single molecule level,<sup>99 90</sup> as well as for many applications in bio-recognition,<sup>125, 126</sup> forensic<sup>127</sup> and analytical sciences.<sup>128 129</sup>

In surface-enhanced Raman spectroscopy (SERS), the enhancement of the electromagnetic (EM) field in the vicinity of the particle depends on many factors such as the nature of metal, the molecule of interest, its interaction with the metallic surface as well as the match between the wavelength of excitation laser and the frequency of the LSPR of the metallic surface or structure.<sup>5, 130</sup>

Similar to Raman, fluorescence can also be enhanced. Fluorescence is very similar to scattering; it involves absorption of a photon, followed by spontaneous emission, which should follow the radiative enhancement when located nearby a metal rough structure or nanostructure. The crucial difference is that scattering (SERS) is instantaneous, while fluorescence is a multi-step process. It means once a photon is absorbed and excites an electron for fluorescence process, no enhancement mechanism can lead to more energy being extracted from this single excited electron, but only energy being extracted faster. The quantum yield cannot be more than 1, and for a dye with a good free-space quantum yield, the only source of enhancement is therefore in absorption cross section.<sup>5</sup>

SEF reaches maximum at a certain distance (10nm or more) from the metal nanostructure, while SERS is highest at the metal surface, a property dubbed the first layer effect.<sup>131</sup> To overcome this problem, and separate the fluorophore from the metal by an appropriate distance, a thin layer over the metal is necessary.<sup>132</sup> In an elegant work led by Tian and co-workers,<sup>92</sup> the protection of gold nanoparticles with an ultrathin layer of  $\text{SiO}_2$ ,  $\text{Al}_2\text{O}_3$ <sup>92</sup> or  $\text{MnO}_2$ <sup>117</sup> is used to isolate the molecules of interest from the surface, thereby preventing direct chemical and electrical contact.

Shell-isolated nanoparticle enhanced Raman spectroscopy (SHINERS) provides a unique way to access the intrinsic molecular fingerprint of the specimen of interest with large enhancement factors.<sup>133</sup> Recently, the use of protected metallic particles has also been shown to be of tremendous interest for enhanced fluorescence, as reported by Aroca

et al.<sup>134,135</sup> Shell-isolated nanoparticles enhanced fluorescence (SHINEF) provides an easy way to avoid the quenching of the fluorophore by the gold surface.<sup>135</sup>

Similarly to SHINERS, the optimization of the materials for SHINEF experiment relies on the proper molecule-metal separation distance, generally in the 10-20 nm range, upon the excitation of the LSPR of the metal. The far-field fluorescence emission of the molecules located around the shell-protected nanoparticles is also modulated by the core size and the shape of the metal particle which opens new tailoring possibilities to address specific spectral regions for analytical purposes.<sup>135</sup> The dominant mechanism in the enhancement of fluorescence from the dye molecule on the silica coated gold nanostructure is attributed to electromagnetic enhancement which results in production of a surface plasmon from the gold nanostructure. As a result, the dye molecule couples efficiently with free charges on the metal surface leading to higher emission intensity.<sup>136,137</sup>

It is noteworthy that most of these recent results, based on shell-protected nanoparticles, have been conducted in colloidal solutions using wet chemistry and bottom-up approaches which provide a reliable size distribution of the protected nanoparticles. The recent work from Gong et al.,<sup>138</sup> has focused on plasmonic-enhanced fluorescence from a single bow-tie nanoaperture milled on an aluminum foil without any shell protection. Although no spatially resolved experiments were performed, the authors measured a remarkable fluorescence enhancement from the single structure which acts as

a “hot-spot” since its LSPR matches both excitation wavelength and fluorescence emission.

Finite difference time domain (FDTD) simulation proved that the fluorescence emission is very sensitive to the input polarization of the excitation light.<sup>139</sup> More importantly, from time-resolved experiments, the decay rate is increased in the vicinity of the single bow-tie assembly demonstrating that each structure can also modulate the lifetime of the fluorophore.<sup>138</sup> Similar work on shell fluorescent nanoparticles reports that the interaction of dye molecules with the metal core greatly magnify the excitation efficiency, enhances the emissive rates, and reduces the lifetime of excited states, resulting in an enhanced photostability and detectability.<sup>38</sup>

In this context, we have investigated the fluorescence enhancement from a collection of SiO<sub>2</sub>-protected gold bow-tie assemblies deposited on a glass surface by nanosphere lithography procedure. The objectives of this work were three fold: first, to evaluate the distribution and the homogeneity of a collection of hot-spots located strictly onto a surface using scanning fluorescence confocal microscopy; second, to tune the dimensions, the interparticle distance and the thickness of the shell of structures in order to obtain maximum fluorescence enhancement, and third, to reveal any polarization effects from these anisotropic structures organized in a hexagonal fashion.

## 4.2 Materials and Methods

### 4.2.1 Reagents

All the reagents were purchased as listed in Chapter 2; section 2.2.1. IRIS-5 dye (water soluble, no reactive group) was obtained from Cyanine Technologies, Settimo Torinese, Italy.

### 4.2.2 Fabrication of nanotriangle arrays

The fabrication of the nanotriangle arrays was performed similar to the procedure outlined in chapter 2, Sections 2.2.2-2.2.5. Briefly, glass coverslips were thoroughly cleaned followed by deposition of polystyrene nanospheres by air- water interface. This sample was allowed to dry overnight and then 3nm of titanium and 30nm of gold was deposited. The polystyrene mask was lifted- off by sonicating the sample in ethanol, creating the nanotriangle array.

### 4.2.3 Sputtering of silica on the substrates

Silica was deposited on the sample using magnetron sputtering system. The sputtering techniques are used to deposit thin films of materials onto a substrate by releasing target atoms from a source through bombardment with energetic ions. In general, the target source is placed onto an electrode, with the application of a large negative voltage to

form a cathode. The target is placed under vacuum and is subsequently exposed to an ionized gas comprised of a mixture of high energy electrons and ions, forming the plasma. The gaseous plasma bombards the target, releasing electrons that contribute to the maintenance of the plasma, and also removing target atoms from the source which become deposited onto a substrate surface.<sup>140</sup>

In order to increase the efficiency of the plasma, magnets are arranged behind the cathode such that a magnetic field, which runs parallel to the target, creates an electron trap.<sup>141</sup> The capture of electrons increases the probability of the electron-atom collisions within the plasma, thereby increasing the plasma density. This translates to an increased deposition rate of atoms onto the substrate, maintenance of the discharge at low pressures ( $10^{-3}$  mbar) with low operating voltages (500V).<sup>140, 142</sup> The main steps of sputtering are shown in Figure 4-1.

When the gold nanotriangles were obtained then different thicknesses of silica (5, 10, 15, 20, 25 nm) were sputtered on the samples. For sputtering silica, the samples were placed in the sample chamber under  $10^{-3}$  mTorr vacuum. The system operates with a source power of 300W, and a chamber pressure of  $10^{-2}$  mbar and an argon flow rate of  $15\text{cm}^3/\text{minute}$ . When the required chamber pressure is obtained, the argon plasma was lit and so the sputtering of silica started. The samples were coated with silica for 5-25 minutes depending on the thickness of silica required.

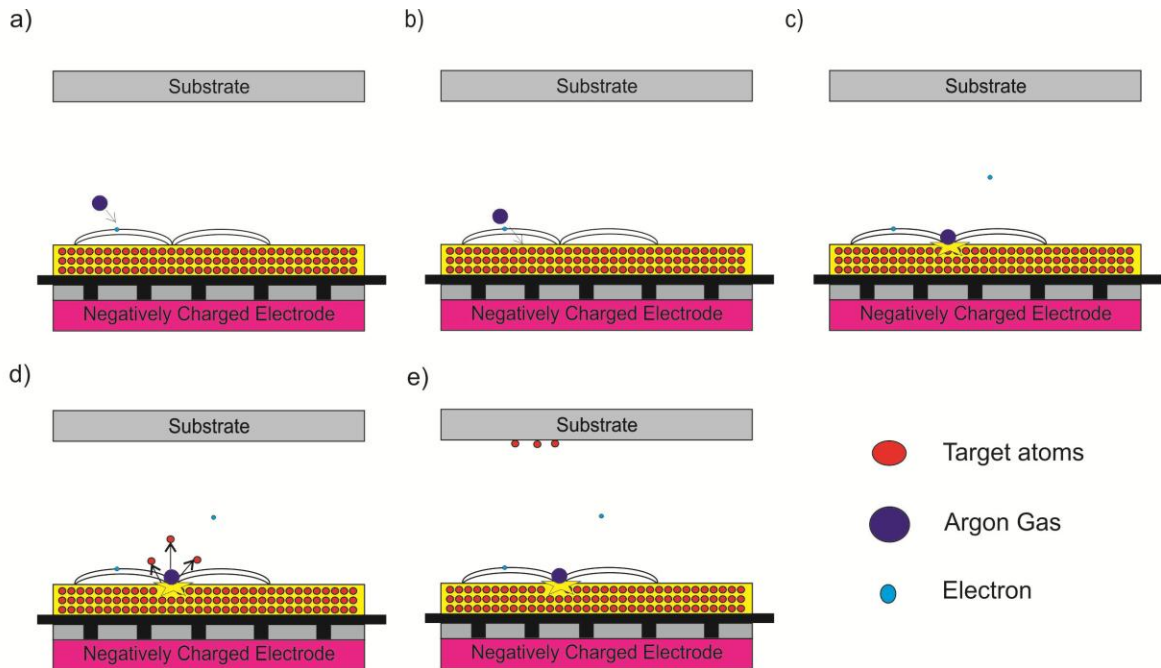


**Figure 4-1** Schematic diagram of the operation of a magnetron sputtering system, a) Argon atoms enter the system and collide with electrons; b) Argon atoms become ionized; c) Ar ions collide with the target surface; d) Target atoms are removed from the surface; e) Target molecules adhere to the substrate surface

## 4.2.4 Imaging the Samples

### 4.2.4.1 Focused ion beam- Scanning electron microscopy (FIB-SEM)

FIB based instruments can be used to section and provide 3D analysis for SEM or FIB imaging. The lower size limit for the FIB slices is found to be of the order of 10nm. The cross sectioning capabilities of FIB provides a precise, site- specific and efficient means for looking below the surface into the bulk of a sample.

Fundamentally, a focused ion beam system produces and directs a stream of high-energy ionized atoms of a relatively massive element focusing them on to the sample for the purpose of milling the surface. The system utilizes a liquid-metal ion source to produce  $\text{Ga}^+$  ions that expel surface atoms from their position to produce secondary electrons from the sample.

This system can be used for four functions: milling, deposition, implantation and imaging. Milling is the process which allows digging into the sample surface using heavy ions as the beam. It can be easily converted to a deposition system by adding a gas delivery device. Its unique property allows it to isolate specific sample regions so that it only makes the necessary modifications to a certain region of the sample without affecting the integrity of the sample as a whole. The combination of FIB with SEM allows the operator to switch from FIB sectioning to SEM observation and back, in matter of seconds.<sup>143</sup>

The thickness of deposited  $\text{SiO}_2$  on the sample was measured using focused ion beam system (FIB-SEM, LEO Zeiss 1540XB FIB/SEM). Thin layers of osmium and platinum were deposited on the sample before carrying out the milling process.

#### 4.2.4.2 Confocal Fluorescence Microscopy

Confocal fluorescence microscopy is a widely used technique that has many advantages as compared to the conventional optical microscope. It can generate high



resolution images, eliminating the out of focus background signal and allowing optical sectioning from thick specimens. The main component of confocal microscopy is the pinhole aperture which removes secondary fluorescence from areas outside of the focal plane and area of interest as a consequence confocal microscopy provides an image with higher resolution and finer details. The illumination of the sample is also different; the entire region of interest is not illuminated but the laser scans across the surface and constructs an image on a point- by-point basis.

The setup for confocal fluorescence microscopy consists of the laser excitation source, directed through the pinhole aperture towards the beam splitting mirror where the light is reflected and focused through the objective onto the sample. As the laser scans across the surface in the defined focal plane, the fluorescence signal is emitted back through the objective and has longer wavelength and it passes through beam splitting mirror towards the second pinhole aperture. It is placed in the front of the photomultiplier tube (PMT) detector that blocks the out- of- plane fluorescence as shown in Figure 4-2. Finally, this data is collected by the computer for acquisition, processing, analysis, and display of images.<sup>144</sup>

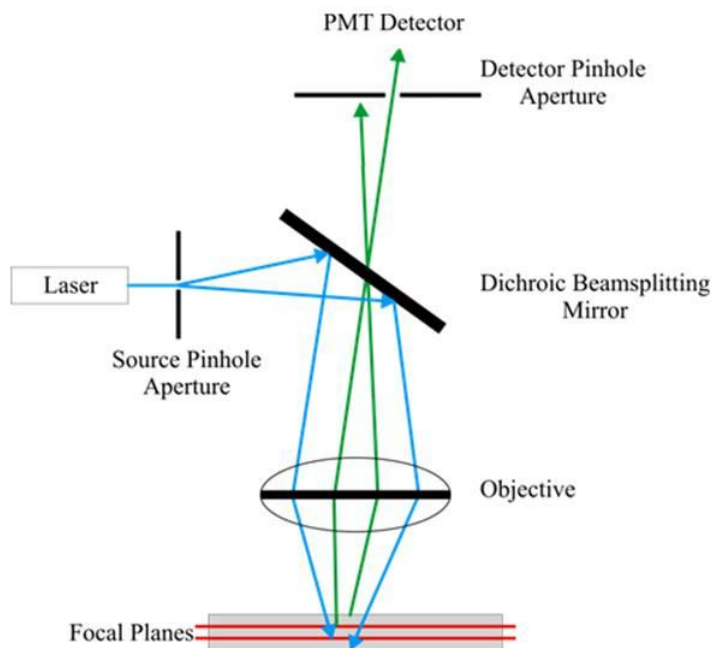


**Figure 4-2** A simplified diagram of the light pathways and important components of the confocal microscope <sup>144</sup>

10  $\mu\text{M}$  solution of IRIS-5 dye was prepared in water. Fluorescence images were collected on Leica Confocal Fluorescence Microscope, TCS SP2 system using 632.8 nm He-Ne laser and oil immersion objective (60 x, 1.32 N.A.). The scanning area for the image was  $512 \times 512$  and the emission of the dye was collected in the range of 650-700 nm. The fluorescence images were obtained before and after adding a drop of the dye on the samples.

## 4.3 Results and Discussion

### 4.3.1 Fabrication of Gold Nanotriangle arrays

The samples were fabricated using NSL followed by e-beam deposition of Au and magnetron sputtering of SiO<sub>2</sub>. Figure 4.3 schematically illustrates the fabrication of gold nanotriangle (GNT) arrays on microscope coverslip. NSL was preferred for the preparation of the samples because it is an inexpensive technique to prepare metal structures over glass surface, has a high throughput, and does not require special apparatus. It can be used to produce nanoparticle arrays with controlled size, shape and interparticle spacing and has been successfully used for SERS experiments.<sup>13, 25, 71</sup>

As discussed previously in section 2.3.1.2., the size and distance between two adjacent nanotriangles can be varied by changing the diameter of the polystyrene microspheres used to prepare sample. This results in surface plasmon resonance observed at 600, 650 and 750 nm for the nanotriangle platforms made with the 0.43, 0.65 and 1.00  $\mu\text{m}$  particles, respectively.

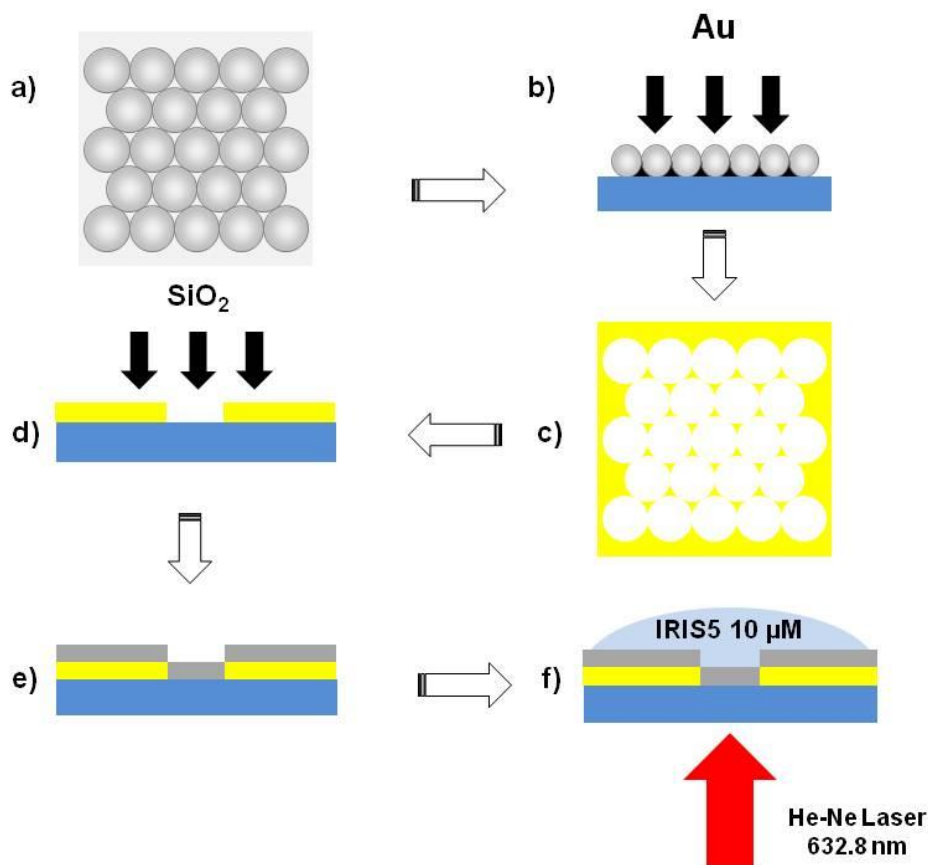


**Figure 4-3** Schematic illustration of experimental procedure; a) top view of polystyrene nanospheres on glass slide, b) deposition of Au, c) top view of nanotriangles after removing polystyrene particles, d) SiO<sub>2</sub> sputtering, e) side view of prepared substrate on coverslip; yellow layer: Au; gray layer: SiO<sub>2</sub>, f) adding a drop of dye (IRIS5 10 μM) on sample and exciting with He-Ne Laser (632.8 nm) for fluorescence measurement

Herein, a thin layer of SiO<sub>2</sub> was deposited on gold nanostructures with varying thicknesses from 5 to 25 nm, to isolate the gold nanotriangles from the fluorescent dye. After the fabrication of samples, fluorescence images were subsequently collected after adding IRIS-5 dye over the platform and these were examined using an inverted confocal

microscope. IRIS-5 absorbs at 647 nm ( $1.8 \times 10^5 \text{ cm}^{-1} \text{ M}^{-1}$ ) and emits at 667 nm (Quantum yield of  $\phi \sim 0.25$ ). Thus a 632.8 nm He-Ne laser was used as the excitation source and the detection range of the detector was set between 650-700 nm.

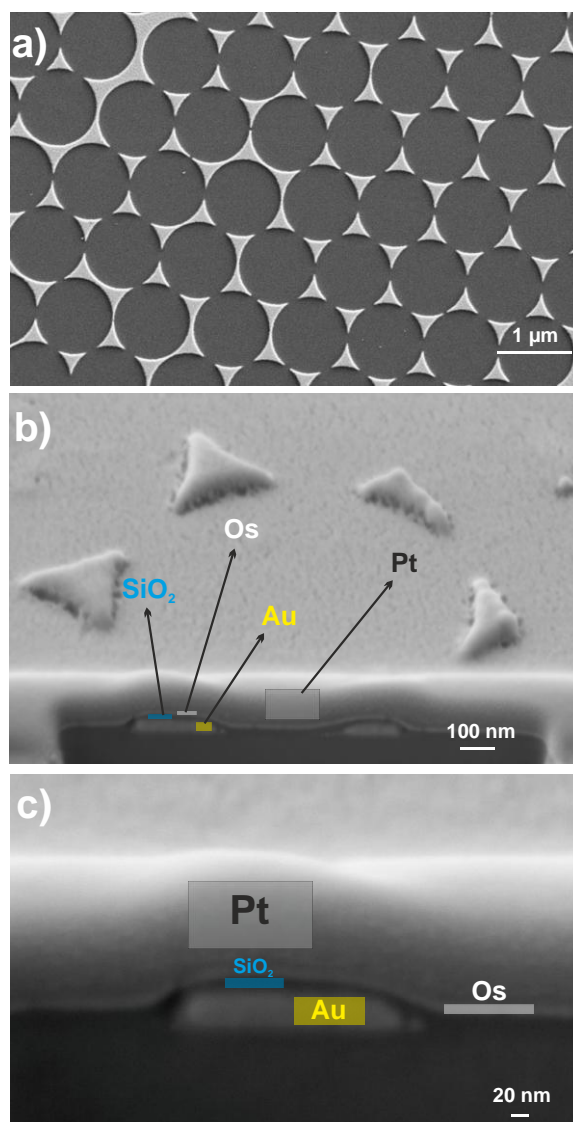


**Figure 4-4** a) SEM image of NSL platform made with 1.00 μm polystyrene nanospheres b) SEM image of the cross-section of a nanotriangle milled using focused ion beam with 20 nm of SiO<sub>2</sub> deposited on top c) The same SEM-FIB image as “b” with higher magnification

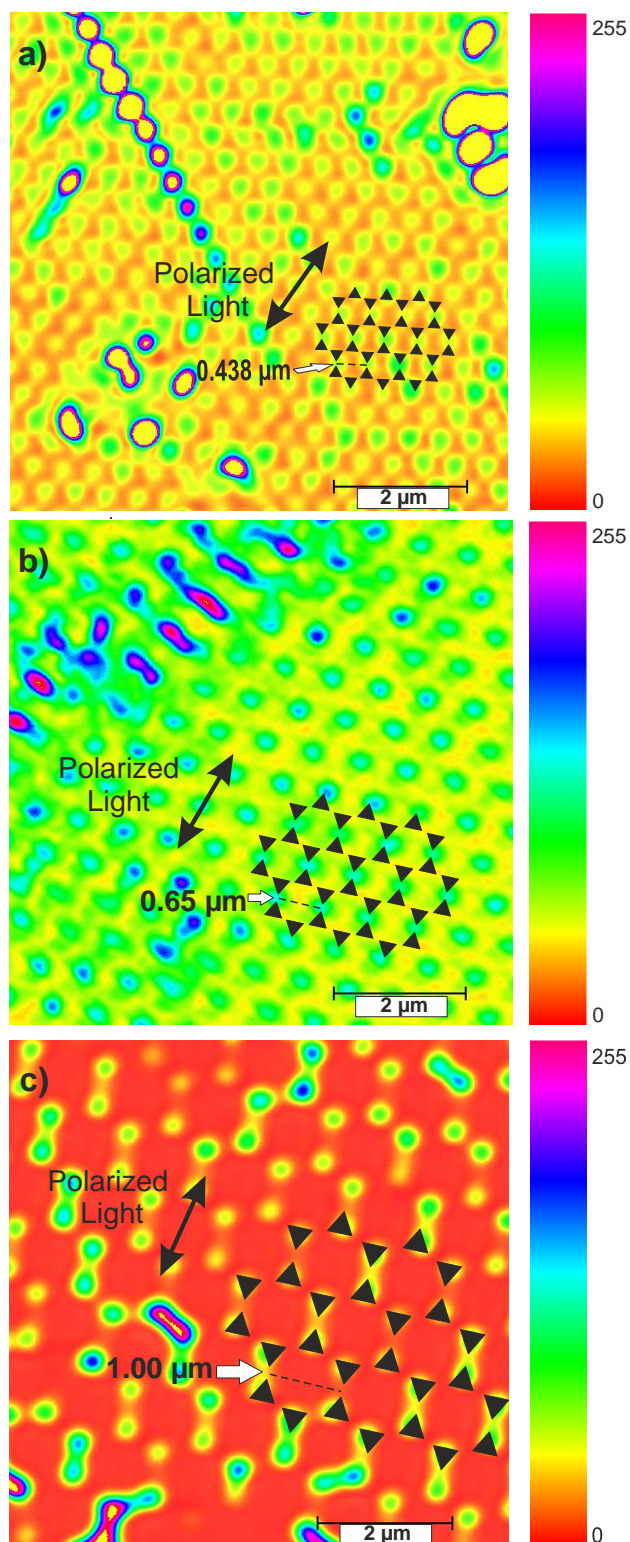
### 4.3.2 Size dependency of nanotriangles on fluorescence enhancement

Figure 4-5 shows a pattern of individual fluorescent hot-spots obtained after adding a droplet of 10  $\mu\text{M}$  solution of dye in water over the  $\text{SiO}_2$ -protected platforms. All the laser-scanning images were subsequently collected with maximum magnification with an (60X, 1.32 NA) oil immersion objective.

The scanning area was typically of  $8 \times 8 \mu\text{m}^2$ . Besides the adjustment of the photomultiplier tube (PMT) settings, the acquisition parameters were the same for all of the samples. In addition, the PMT voltage was adjusted depending on the efficiency of the fluorescence.

It has been previously shown by theoretical calculation that production of LSPR results in the generation of “hot-spots” at the apex between two adjacent nanotriangles. It was also proven that this phenomenon was dependent on the polarization direction of the impinging light and the hot-spots showed maximum electromagnetic enhancement when the polarized field is parallel to the bow tie axis.<sup>123, 138, 145</sup>

However, it has never been shown how homogeneous was the distribution of the hot-spots over the surface. Hence, mapping the distribution of hotspots is of great interest to 1) improve the density of hot-spots for a given probing method and 2) localize accurately the areas over a surface that are most efficient to enhance both the input and output electromagnetic fields.



**Figure 4-5** Fluorescence images showing individual “hot-spots” on GNT arrays after adding the dye: a) 0.43  $\mu\text{m}$  b) 0.65  $\mu\text{m}$  c) 1.00  $\mu\text{m}$

Reported in Figure 4-5, the nanotriangles are drawn to scale over the fluorescence patterns so that the concept mentioned previously can be proved. In this work, SEF was mainly observed for the bow-tie assemblies that were parallel to the polarization axis of the input excitation light while no enhancement was observed for nanotriangles which were perpendicular to the axis of the polarization. It is noteworthy that the fluorescence pattern observed in Figure 4-5c shows only a hexagonal type structure as opposed to Figure 4-5 a-b that shows a centered hexagonal structure. In the case of 1.00  $\mu\text{m}$  particles, Figure 4-5 c shows the back reflection of the excitation laser from the nanotriangles. In the latter case, no SEF is observed due to the non-matching conditions between the LSPR of the platform and the excitation source. Figure 4-5 a-b shows clearly that at each bow-tie assembly oriented along the polarization direction, a well localized enhanced fluorescence spot can be clearly seen with large intensity and contrast.

For the two smaller triangles structures, the polarization dependent fluorescence GNT arrays display a hexagonal centered pattern upon addition of the dye solution as shown in Figure 4-6. Figure 4-6 a-b shows the fluorescence hot-spots before and after adding the dye. When the dye is not present on the structure (Figure 4-6c) the probe laser is simply back reflected from the gold individual triangles and the long-pass filter of the apparatus is not efficient enough to completely remove the Rayleigh back-scattering of the excitation light. There is no fluorescence background and the shape of the individual triangles, although in the 200 nm range, can be distinguished in Figure 4-6 c. As soon as the dye is added on the GNT arrays, a pronounced enhancement in the fluorescence is observed as seen in Figure 4-6 d. The enhancement occurs only at the junctions between



opposite nanotriangles and has much greater fluorescence intensity as compared to the background. In all the three samples, fluorescence was most enhanced for  $0.65\ \mu\text{m}$ , followed by  $0.43\ \mu\text{m}$  NSL platforms.

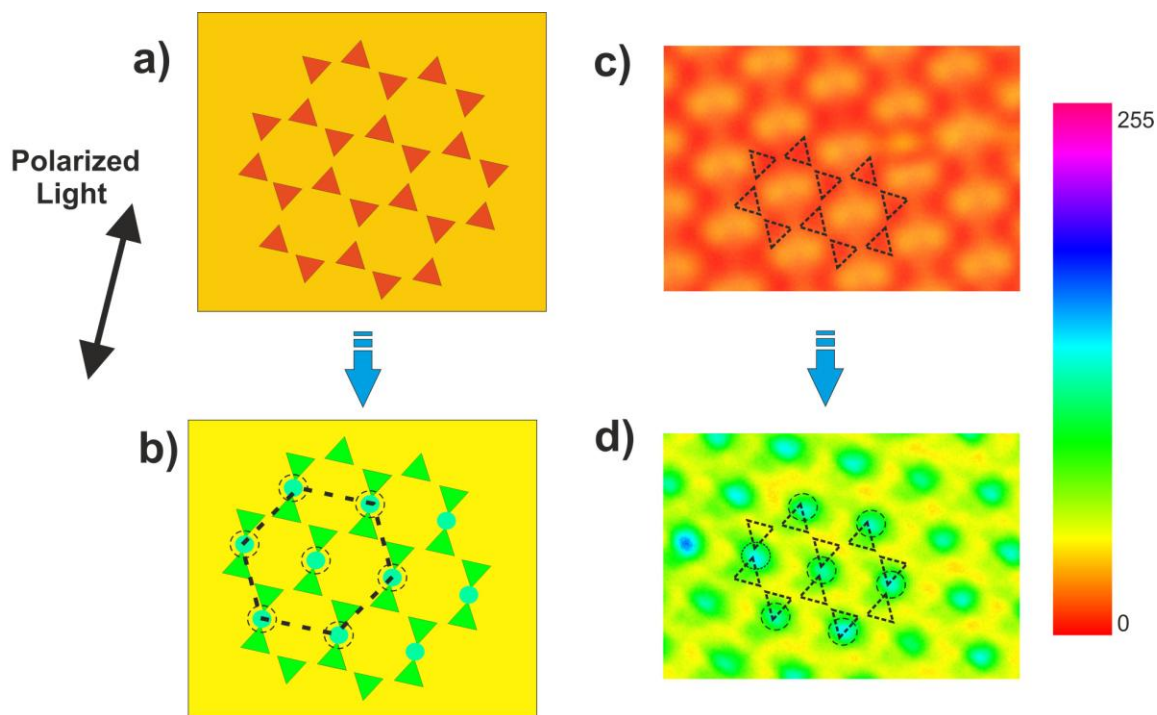


**Figure 4-6** Illustration of: a) the model of GNT arrays before adding the dye, b) the model of individual hot-spots after adding the dye, c) fluorescence image of  $0.65\ \mu\text{m}$  GNT arrays with 25 nm silica on top before adding the dye, d) mapping individual hot-spots after adding the dye on the same fluorescence image demonstrated in c

A surface fluorescence enhancement factor (SFEF) can be estimated using the color-coded fluorescence intensity map reported in Figure 4-6 d. After adding the dye, the individual hotspots appeared which had a higher intensity represented by a blue color. The background (yellow color) corresponds to the intrinsic fluorescence of the dye-solution without any surface effect. The fluorescence intensity originating from the hot-

spots is roughly twice the intensity of the non-enhanced fluorescence. These values can be compared with those reported by Aroca et al. who reported 10-fold absolute average enhancement from colloidal solution of gold nanorods (40 nm) protected with 11 nm of silica.<sup>135</sup> Chi et al. reported the enhancement of 2.8-fold observed on randomly distributed silica nanoparticles as well as 16 and 6-folds for 500-nm-dot and  $6 \times 6 \mu\text{m}^2$  silver nanoparticle arrays, respectively.<sup>146</sup> Similarly, the enhanced fluorescence intensity of about 3.2-fold within isolated bow-tie nano-apertures was also reported by Gong et al.<sup>138</sup> and is within the same order of magnitude compared to our results.

To estimate the SFEF, one must calculate the number of molecules experiencing the enhanced EM field. Alternatively, we can use the volume subject to local enhancement and compare it to the focal volume on the bare glass surface (i.e. outside a bow-tie assembly). A typical focal volume using a high N.A. objective is roughly about  $V_F = 1 \mu\text{m}^3$ . For single bow-tie antennae, the volume can be approximated using the separation distance between two adjacent nanotriangles  $d_{t-t}$ , as well as the typical dimension of a single triangle apex length ( $l_t$ ) and thickness of the structure ( $d_z$ ). The volume will be roughly about

$$V_{SFEF} = d_{t-t} \times l_t \times d_z = (150 \times 30 \times 58) \text{nm}^3 = 2.61 \times 10^{-4} \mu\text{m}^3 \quad (4.1)$$

Using the fluorescence intensities from two areas (enhanced ( $I_{SFEF}$ ) and non-enhanced ( $I_F$ ) and the volume involved, the SFEF can be estimated using the following equation:

$$SFEF = \frac{V_F}{V_{SFEF}} \times \frac{I_{SFEF}}{I_F} = \frac{1}{2.61 \times 10^{-4}} \times 2 = 7.7 \times 10^4 \quad (4.2)$$

The enhancement factor was determined for the sample made with 0.65  $\mu\text{m}$  particles and coated with 25 nm silica. This is a rough estimation from a single hot-spot and several factors such as focal region, number of hot-spots, intensity of hot-spots, apex size, the thickness of gold and silica were considered. Thus, the order of magnitude of the surface-enhanced fluorescence is in the range of  $10^3$ - $10^4$  for such surface assuming that only one hot-spot is probed at the time. If we assume that we have 6 hotspots in the focal region, the enhancement factor will be reduced to  $1.4 \times 10^3$ .

As the size, shape and environment of the sample changes, the LSPR of the surface is also altered. Besides, variation in the thickness of deposited silica played a major role by affecting the fluorescence enhancement.<sup>33, 147</sup> The enhancement factor (EF) of metal-enhanced fluorescence (MEF) is dependent on enhanced absorption and emission. Furthermore, the enhanced absorption is related to the overlap of the surface plasmon resonance (SPR) of the nanoparticles and absorption band of fluorophores, resulting in high emission. The latter factor changes the quantum yield and lifetime of the fluorophore.<sup>136, 146</sup>

The SEM image of 0.43 $\mu\text{m}$  nanospheres with higher magnification is shown in Figure 4-7 a. The same size of nanospheres was used in Figure 4-7 b and c to demonstrate the difference between the areas with leftover nanospheres and nanotriangles in terms of fluorescence intensity. In these figures, the areas demarcated with black dotted lines indicate the areas with polystyrene nanospheres while the rest of the sample contains nanotriangles. In both of these images, the area with nanospheres shows greater fluorescence intensity as compared to the area with the nanotriangles. This is the result of the lens effect of the nanoparticles that in turn focused the incoming light as shown in

Figure 4-8.<sup>148</sup> The lens effect is the ability of the polystyrene particles to focus the incident laser (632.8 nm) resulting in higher intensity spots.

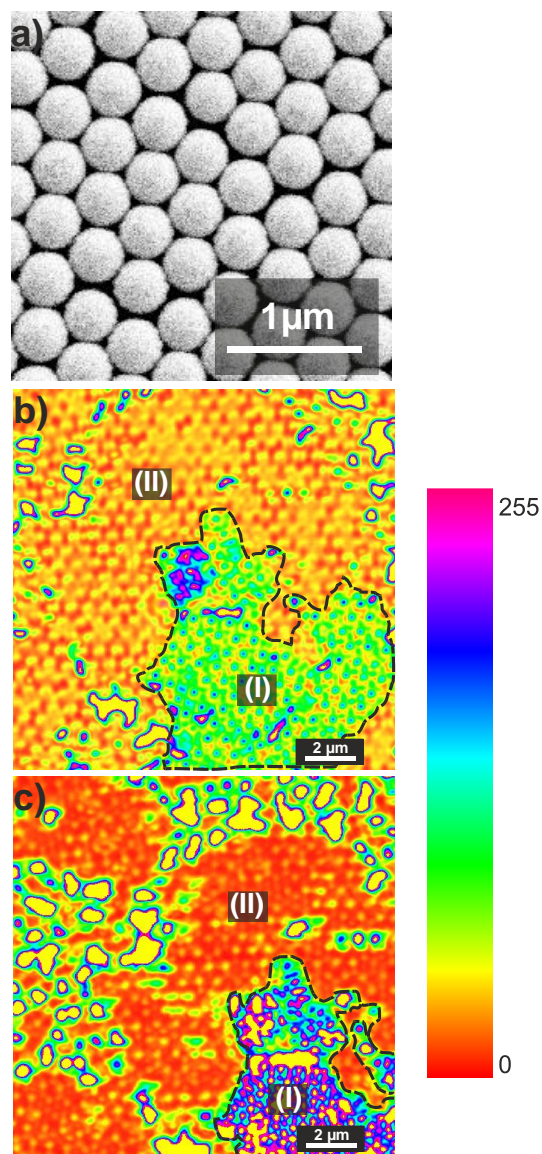


**Figure 4-7** a) SEM image of 0.43 μm polystyrene monolayer, b) fluorescence image of GNT arrays (II) along with 0.43 nanospheres (I) without dye, c) fluorescence image of GNT arrays (II) along with 0.43 nanospheres (I) with dye

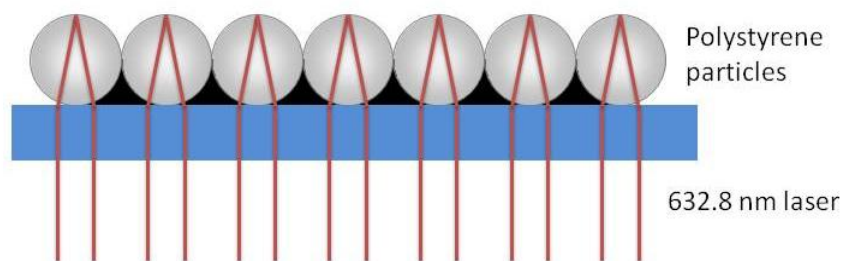


**Figure 4-8** The lens effect when the incoming light is focused on to the polystyrene nanospheres

#### 4.3.3 Effect of SiO<sub>2</sub> thickness on fluorescence enhancement

It has long been known that the presence of a nanostructured metal can affect the fluorescence properties of a nearby fluorophore. Depending on the distance and geometry between the fluorophore and the metal, the fluorescence emission can be enhanced or quenched. Hence, metallic nanostructures must be protected by a thin non-metallic shell such as SiO<sub>2</sub> to avoid fluorescence quenching.<sup>131,4</sup> Besides, it has been shown that the fluorophore must be at least 5–10 nm away from the metal surface for surface enhancement.<sup>36, 149-151</sup>

Most of the published research in SEF is done on nanostructures<sup>152-154</sup> or on single nanoparticles.<sup>35, 155-158</sup> To the best of our knowledge, SEF has never been reported for GNT arrays. In practice, there are several factors that may influence the final observable SEF EF. These factors - random orientation and position distribution of GNTs compared to excitation polarization-cause a large reduction in the excitation enhancement and decay rate enhancement, with only a small effect on the non-radiative decay rate.<sup>159</sup>

In this work, the GNT arrays with various thickness of SiO<sub>2</sub> (5 to 25 nm) were studied. The enhancement for 0.65 and 0.43 μm GNT arrays was the best seen in 25 and 5 nm of silica, respectively. Enhancement was also observed for GNT arrays with 10, 15, and 20 nm of silica as well.

## 4.4 Conclusion

In summary, we have demonstrated that GNT arrays can be fabricated by NSL and then with gold and silica deposition for Surface-Enhanced Fluorescence (SEF). The intensity of SEF can be tuned by changing the diameter of polystyrene nanospheres used to prepare the samples, which is related to the LSPR of the GNT arrays and the emission range of the dye used. It was also proved that the nanotriangles parallel to the axis of the polarized light exhibit electromagnetic enhancement to produce individual “hot-spots”. Effect of different thicknesses of silica was also considered and the thickness that worked best for each sample was found out. It is noteworthy that the triangle separation can be reduced to obtain more compact structures which could result in the generation of the hot-spots with even higher fluorescence enhancement due to the ideal matching conditions between the LSPR and excitation source.

## Chapter 5

### 5 Summary and Future Prospectives

This chapter presents the brief-overview of method, i.e. nanosphere lithography, used to fabricate platforms for enhancing the Raman and fluorescence signal. The prospects for the future studies involve the modification of samples produced by nanosphere lithography technique by reactive ion etching (RIE) to enhance the versatility of this technique.

#### 5.1 Summary

Various nanofabrication techniques such as e-beam lithography and photolithography produce metallic nanostructures that can be used to enhance Raman or fluorescence signals via an electromagnetic enhancement mechanism. To this end, it is necessary that the excitation wavelength matches the LSPR of the substrate produced. The size and the shape of the nanostructures also play a major role in tuning the LSPR. The disadvantages of the above mentioned techniques are cost and need for expensive equipment to make the metallic nanostructure. The main advantage of nanosphere lithography is that it is an inexpensive and fast technique which can be used to make metallic nanostructures easily.

In this thesis, nanosphere lithography was employed to make substrates with efficient enhancement capabilities for both Raman and fluorescence applications. The



fabrication and characterization of samples is discussed in detail in Chapter 2, wherein the combination of nanosphere lithography followed by gold deposition and lift-off was used. This process led to form large areas ( $>100\mu\text{m}^2$ ) of nanotriangle arrays. The size of the nanotriangles and the gap between them can be varied by changing the diameter of the polystyrene particles used to make the sample. The samples were characterized by optical microscopy, scanning electron microscopy (SEM), atomic force microscopy (AFM) and then followed by the determination of the extinction spectrum to find out the working wavelength of the sample. Results indicated that after the lift-off, there was no polystyrene mask present on the sample. It was found that the size of the nanotriangles varied by changing the diameter of polystyrene mask. Defects such as polydispersity, point randomness, line defects were also observed.

To assess the efficiency of the nanotriangle, the Raman spectrum of benzenethiol and azobenzene thiol<sup>25</sup> was recorded and is discussed in Chapter 3. It was observed that SERS signal can be tuned by changing the diameter of polystyrene nanospheres used to prepare the samples, which is related to the matching LSPR of the sample with the excitation laser. The assignment of the vibrational modes of the molecules was in accordance with values reported in literature. The SERS spectrum was obtained at low laser intensity and acquisition time. It is noteworthy that absolutely no enhancement of signal was observed on plain flat (non-structured) gold.

Finally, in Chapter 4, the substrate made by nanosphere lithography followed by gold deposition, lift-off and then silica deposition can be used for fluorescence enhancement along with a fluorophore. It was observed that the intensity of SEF can be tuned by changing the diameter of polystyrene nanospheres used to prepare the samples, which is

related to the LSPR of the gold nanotriangle arrays and the emission range of the dye used. It was also proved that the enhancement was dependent on the axis of polarized light which is conjunction to the results reported for in the FDTD calculations in other studies.<sup>123</sup> It was found that the nanotriangles parallel to the axis of the polarized light exhibit electromagnetic enhancement to produce individual “hot-spots”. The effect of different thicknesses of silica was also considered and the thickness that worked best for each sample was found out.

It has been proved that the substrates made by nanosphere lithography were efficient in enhancing the Raman and fluorescence signal of a molecule or a fluorophore. The ease of the nanosphere lithography technique presents an opportunity to be widely used in the laboratory with control on the size and interparticle distance.

## 5.2 Future Prospects

Nanosphere lithography was utilized in this thesis for making the nanotriangles to enhance the Raman and fluorescence signal. The polystyrene nanosphere monolayer acts as a mask and then this is followed by gold deposition and then the lift-off. In this thesis, nanotriangle arrays have been produced but with certain modifications, this technique can be used to produce nanohole arrays.<sup>75</sup> This will help change the LSPR of the sample, making it possible to work at other excitation wavelength ranges as well.

One of the goals of our research group is to apply SERS measurements to the study of chemical exchanges between the cells such as neurons. First it is necessary to grow the biological cell over the SERS platform. This can be achieved by variety of methods such as microcontact printing, self assembly and dip pen lithography have been used to accurately position cells. For these techniques, the surfaces need to be patterned with proteins or alkane thiols to either prevent or promote cell adhesion in certain regions across the surface. The approach developed in our group is to use a thin film of fluoropolymer to guide the growth of cells and make sure they are positioned over the SERS platforms. A fluorocarbon was chosen due to its wide range of physical and chemical properties as well as its non adhesive properties to cells. When mammalian cells were grown on this substrate, it was observed that the cells exclusively grew within the glass exposed areas while avoiding the polymer background. The microscope coverslips were patterned using photolithography, followed by plasma deposition of single thin polymer film and then followed by lift-off.<sup>160</sup> Figure 5-1 shows the fluorescent image of a single myoblast cell cultured on the fluoropolymer patterned substrate.

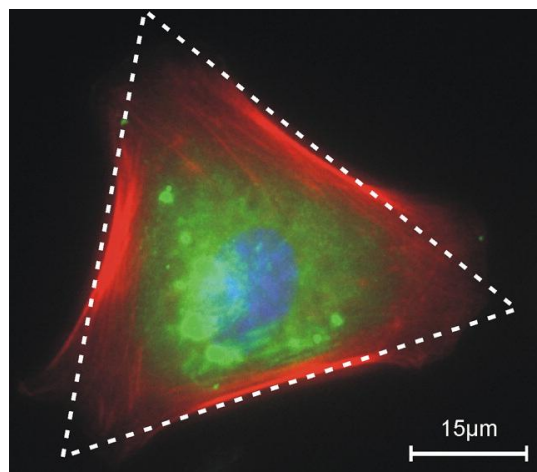


**Figure 5-1** Fluorescent image of a myoblast cell cultured in single cell patterning<sup>160</sup>

In a second step, these substrates can be used in conjunction with nanosphere lithography which can then be used to make the SERS pattern on this substrate. Figure 5-2 a shows the fluoropolymer patterned substrate with polystyrene nanospheres while figure 5-2 b depicts the substrate after gold deposition followed by lift-off. This substrate can be used to grow healthy and cancerous mammalian cells and then record the SERS spectra for each type respectively. The Raman or fluorescence signal from biological material will be identified and compared for healthy and cancer cells. This will be of interest for the early detection of the disease's markers.

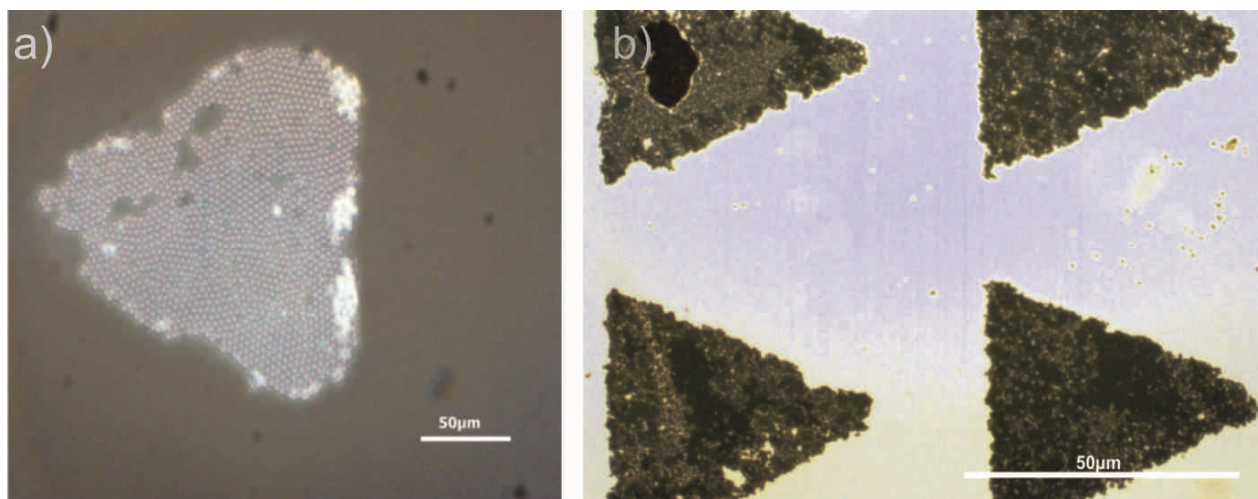


**Figure 5-2** a) Optical image of fluoropolymer patterned substrate with polystyrene nanospheres (1.00 μm) taken with 100 x objective (N.A.0.95), b) optical image taken with 20x objective (N.A.0.5) of the same substrate followed by gold deposition and then lift-off

It is noteworthy that the triangle separation can be reduced by reactive ion etching (RIE) to obtain more compact structures which could result in the generation of the hot-spots with even higher fluorescence enhancement due to the ideal matching conditions

between the LSPR and excitation source. Similarly, it will also be interesting to study the enhancement of fluorescence in the case of the silver nanotriangles protected with silica and to compare the enhancement factors in both the cases.

## 5.3 References

1. Vo-Dinh, T., *TrAC, Trends Anal. Chem.* **1998**, *17*, 557-581.
2. Petry, R.; Schmitt, M.; Popp, J., *Chem. Phys. Chem.* **2003**, *4*, 14-30.
3. Smith, E.; Dent, G.; Wiley, J. In *Modern Raman spectroscopy: a practical approach*, John Wiley & Sons Ltd, 2005, pp 1-2.
4. Li, W.; Zhang, J.; Zhou, Y.; Zhang, P., *Chem. Commun.* **2011**, *47*, 5834-5836.
5. Le Ru, E. C.; Etchegoin, P. G. In *Principles of Surface-Enhanced Raman Spectroscopy: and related plasmonic effects*, Elsevier, Oxford, U.K, 2009.
6. Fleischmann, M.; Hendra, P. J.; McQuillan, A. J., *Chem. Phys. Lett.* **1974**, *26*, 163-166.
7. Hering, K.; Cialla, D.; Ackermann, K.; Dörfer, T.; Möller, R.; Schneidewind, H.; Matheis, R.; Fritzsche, W.; Rösch, P.; Popp, J., *Anal. Bioanal. Chem.* **2008**, *390*, 113-124.
8. Stiles, P. L.; Dieringer, J. A.; Shah, N. C.; Van Duyne, R. P., *Annu. Rev. Anal. Chem.* **2008**, *1*, 601-626.
9. Moskovits, M. In *Surface-Enhanced Raman Scattering: Physics and Applications*, Kneipp, K.; Moskovits, M.; Kneipp, H., Eds. Springer, Berlin, Germany, 2006, Vol. 103, p 1.
10. Liberman, V.; Yilmaz, C.; Bloomstein, T. M.; Somu, S.; Echegoyen, Y.; Busnaina, A.; Cann, S. G.; Krohn, K. E.; Marchant, M. F.; Rothschild, M., *Adv. Mater.* **2010**, *22*, 4298-4302.
11. Alexander, K. D.; Skinner, K.; Zhang, S. P.; Wei, H.; Lopez, R., *Nano Lett.* **2010**, *10*, 4488-4493.

12. Ito, T.; Okazaki, S., *Nature* **2000**, *406*, 1027-1031.
13. Haynes, C. L.; and Van Duyne, R. P., *J. Phys. Chem. B* **2001**, *105*, 5599-5611.
14. Link, S.; El-Sayed, M. A., *Annu. Rev. Phys. Chem.* **2003**, *54*, 331-366.
15. Kelly, K. L.; Coronado, E.; Zhao, L. L.; Schatz, G. C., *J. Phys. Chem. B* **2003**, *107*, 668-677.
16. Jain, P. K.; Lee, K. S.; El-Sayed, I. H.; El-Sayed, M. A., *J. Phys. Chem. B* **2006**, *110*, 7238-7248.
17. Willets, K. A.; and Van Duyne, R. P., *Annu. Rev. Phys. Chem.* **2007**, *58*, 267-297.
18. Moskovits, M., *J. Raman Spectrosc.* **2005**, *36*, 485-496.
19. Murray, W. A.; Barnes, W. L., *Adv. Mater.* **2007**, *19*, 3771-3782.
20. Kerker, M.; Wang, D. S.; Chew, H., *Appl. Opt.* **1980**, *19*, 4159-4174.
21. Schlücker, S., *Phys. Chem. Chem. Phys.* **2009**, *10*, 1344-1354.
22. Arenas, J. F.; Lopez-Tocon, I.; Castro, J. L.; Centeno, S. P.; Lopez-Ramirez, M. R.; Otero, J. C., *J. Raman Spectrosc.* **2005**, *36*, 515-521.
23. Otto, A., *J. Raman Spectrosc.* **2005**, *36*, 497-509.
24. Dietzek, B.; Cialla, D.; Schmitt, M.; Popp, J. In *Confocal Raman Microscopy*, Dieing, T.; Hollericher, O.; Toporski, J., Eds. Springer, Berlin, 2010.
25. Marquestaut, N.; Martin, A.; Talaga, D.; Servant, L.; Ravaine, S.; Reculosa, S.; Bassani, D. M.; Gillies, E.; Lagugné-Labarthet, F., *Langmuir* **2008**, *24*, 11313-11321.
26. Pergolese, B.; Muniz-Miranda, M.; Bigotto, A., *J. Phys. Chem. B* **2004**, *108*, 5698-5702.

27. Zhu, T.; Fu, X.; Mu, T.; Wang, J.; Liu, Z., *Langmuir* **2003**, *15*, 5197-5199.
28. Zhao, L.; Kelly, K. L.; Schatz, G. C., *J. Phys. Chem. B* **2003**, *107*, 7343-7350.
29. Lu, X.; Rycenga, M.; Sykrabalak, S. E.; Wiley, B.; Xia, Y., *Annu. Rev. Phys. Chem.* **2009**, *60*, 167-192.
30. Mock, J. J.; Barbic, M.; Smith, D. R.; Schultz, D. A.; Schultz, S., *J. Phys. Chem.* **2002**, *116*, 6755-6759.
31. Camargo, P. H. C.; Cobley, C. M.; Rycenga, M.; Xia, Y., *Nanotechnology* **2009**, *20*, 1-8.
32. Jensen, T. R.; Schatz, G. C.; Van Duyne, R. P., *J. Phys. Chem. B* **1999**, *103*, 2394-2401.
33. Henry, A.-I.; Bingham, J. M.; Ringe, E.; Marks, L. D.; Schatz, G. C.; Van Duyne, R. P., *J. Phys. Chem. C* **2011**, *115*, 9291-9305.
34. Philpott, M. R., *J. Chem. Phys.* **1975**, *62*, 1812-1817.
35. Tam, F.; Goodrich, G. P.; Johnson, B. R.; Halas, N. J., *Nano Lett.* **2007**, *7*, 496-501.
36. Anger, P.; Bharadwaj, P.; Novotny, L., *Phys. Rev. Lett.* **2006**, *96*, 113002-113006.
37. Dulkeith, E.; Morteani, A. C.; Niedereichholz, T.; Klar, T. A.; Feldmann, J.; Levi, S. A.; van Veggel, F. C. J. M.; Reinhoudt, D. N.; Möller, M.; Gittins, D. I., *Phys. Rev. Lett.* **2002**, *89*, 203002-203006.
38. Brouard, D.; Viger, M. L.; Guillermo Bracamonte, A.; Boudreau, D., *ACS Nano* **2011**, *5*, 1888-1896.
39. Suhling, K.; Siegel, J.; Phillips, D.; French, P. M. W.; Lévêque-Fort, S.; S.E.D, W.; Davis, D. M., *Biophys. J.* **2002**, *83*, 3589-3595.



40. Fort, E.; Grésillon, S., *J. Phys. D: Appl. Phys.* **2008**, *41*, 013001-013031.
41. Zhao, J.; Jensen, L.; Sung, J.; Zou, S.; Scharzt, G. C.; van Duyne, R. P., *J. Am. Chem. Soc.* **2007**, *129*, 7647-7656.
42. Lombardi, J. R.; Birke, R. L.; Lu, T.; Xu, J., *J. Chem. Phys.* **1986**, *84*, 4174-4182.
43. Fuchs, R.; Barrera, R. G., *Phys. Rev. B* **1981**, *24*, 2940-2950.
44. Beellesa, J.; Bonnand, C.; Plenet, J.; Mugnier, J., *Phys. Rev. Lett.* **2004**, *93*, 036404-036408.
45. Gong, J.; Lipomi, D. J.; Deng, J.; Nie, Z.; Chen, X.; Randall, N. X.; Nair, R.; Whitesides, G. M., *Nano Lett.* **2010**, *10*, 2702-2708.
46. Eustis, S.; El-Sayed, M. A., *Chem. Soc. Rev.* **2006**, *35*, 209-217.
47. Zheng, C. In *Micro-Nanofabrication*, Springer-Verlag Beijing, 2005, pp 15, 77-78.
48. Healy, K. E.; Thomas, C. H.; Rezanian, J. E.; Kim, P. J.; Mckeown, J.; Lom, B.; Hockberger, P. E., *Biomaterials* **1996**, *17*, 195-208.
49. Lee, J. Y.; Shah, S. S.; Zimmer, C. C.; Lui, G.; Rezvin, A., *Langmuir* **2008**, *24*, 2232-2239.
50. Dinish, U. S.; Yaw, F. C.; Agarwal, A.; Olivo, M., *Biosens. Bioelectron.* **2010**, *26*, 1987-1992.
51. Tan, R. Z.; Agarwal, A.; Balasubramanian, N.; Kwong, D. L.; Jiang, Y.; Widjaja, E.; Garland, M., *Sens. Actuators, A* **2007**, *139*, 36-41.
52. El-Sayed, I. H.; Huang, X.; El-Sayed, M. A., *Nano Lett.* **2005**, *5*, 829-834.
53. Bardhan, R.; Grady, N. K.; Cole, J. R.; Joshi, A.; Halas, N. J., *ACS Nano* **2009**, *3*, 744-752.

54. Lohmueller, T.; Iversen, L.; Schmidt, M.; Rhodes, C.; Tu, H. L.; Lin, W. C.; Groves, J. T., *Nano Lett.* **2012**, DOI:10.1021/nl300294b.
55. Xu, Z.; Hao, J.; Braida, W.; Strickland, D.; Li, F.; Meng, X., *Langmuir* **2011**, *27*, 13773-13779.
56. Wustholz, K. L.; Brosseau, C. L.; Casadio, F.; Van Duyne, R. P., *Phys. Chem. Chem. Phys.* **2009**, *11*, 7350-7359.
57. Wallraff, G. M.; Hinsberg, W. D., *Chem. Rev.* **1999**, *99*, 1801-1821.
58. Duan, H.; Fernández-Domínguez, A. I.; Bosman, M.; Maier, S. A.; Yang, J. K. W., *Nano Lett.* **2012**, *12*, 1683-1689.
59. Roder, H.; Hahn, E.; Brune, H.; Bucher, J.-P.; Kern, K., *Nature* **1993**, *366*, 141-143.
60. Li, A.; Liu, F.; Petrovykh, D. Y.; Lin, J.-L.; Viernow, J.; Himpsel, F. J.; Lagally, M. G., *Phys. Rev. Lett.* **2000**, *85*, 5380-5383.
61. Zach, M. P.; Ng, K. H.; Penner, R. M., *Science* **2000**, *290*, 2120-2123.
62. McClelland, J. J.; Scholten, R. E.; Palm, E. C.; Celotta, R. J., *Science* **1993**, *262*, 877-880.
63. Deckman, H. W.; Dunsmuir, J. H., *Appl. Phys. Lett.* **1982**, *41*, 377-379.
64. Fischer, U. C.; Zingsheim, H. P., *J. Vac. Sci. Technol.* **1981**, *19*, 881-885.
65. Haes, A. J.; Van Duyne, R. P., *J. Am. Chem. Soc.* **2002**, *124*, 10596-10604.
66. Xia, Y.; Gates, B.; Li, Z. Y., *Adv. Mater.* **2001**, *13*, 409-413.
67. Velev, O. D.; Tessier, P. M.; Lenhoff, A. M.; Kaler, E. W., *Nature* **1999**, *401*, 548-548.
68. Hulteen, J. C.; Van Duyne, R. P., *J. Vac. Sci. Technol. A* **1995**, *13*, 1553-1558.

69. Yang, S.-M.; Jang, S. G.; Choi, D.-G.; Kim, S.; Yu, H. K., *Small* **2006**, *2*, 458-475.
70. Kosiorek, A.; Kandulski, W.; Glaczynska, H.; Giersig, M., *Small* **2005**, *1*, 439-444.
71. Yu, J.; Yan, Q.; Shen, D., *Appl. Mater. Interfaces* **2010**, *2*, 1922-1926.
72. Wang, D.; Möhwald, H., *Adv. Mater.* **2004**, *16*, 244-247.
73. Retsch, M.; Zhou, Z.; Rivera, S.; Kappl, M.; Zhao, X. S.; Jonas, U.; Li, Q., *Macromol. Chem. Phys.* **2009**, *210*, 230-241.
74. Tsai, P. S.; Yang, Y. M.; Lee, Y. L., *Langmuir* **2006**, *22*, 5660-5665.
75. Murray-Methot, M.-P.; Menegazzo, N.; Masson, J. F., *Analyst* **2008**, *133*, 1714-1721.
76. Huang, Z. P.; Carnahan, D. L.; Rybczynski, J.; Giersig, M.; Sennett, M.; Wang, D. Z.; Wen, J. G.; Kempa, K.; Ren, Z. F., *Appl. Phys. Lett.* **2003**, *82*, 460-463.
77. Pieranski, P., *Phys. Rev. Lett.* **1980**, *45*, 596-572.
78. Cheng, L.; Hong, G.; Qi, L., *Chem. Mater* **2010**, *22*, 476-481.
79. Cheung, C. L.; Nikoli, R. J.; Reinhardt, C. E.; Wang, T. F., *Nanotechnology* **2006**, *17*, 1339-1343.
80. Wang, X.; Xu, S.; Cong, M.; Li, H.; Gu, Y.; Xu, W., *Small* **2012**, DOI: 10.1002/sml.201102274.
81. Chang, Y.-C.; Wang, S.-M.; Chung, H.-C.; Chung-Bin, T.; Chang, S.-H., *Plasmonics* **2011**, *6*, 599-604.
82. Ruan, W.; Lu, Z.; Zhou, T.; Zhao, B.; Nui, L., *Anal. Methods* **2010**, *2*, 684-687.
83. Movchan, B. A., *Surf. Eng.* **2005**, *22*, 35-46.

84. Prasad, P. N. In *Nanophotonics*, John Wiley & Sons Ltd, 2004, pp 195-197.
85. Egerton, R. F. In *Physical Principles of Electron Microscopy*, Springer Science Inc., New York, 2005, p 125.
86. Braga, P. C.; Ricci, D. In *Atomic force microscopy : biomedical methods and applications*, Braga, P. C.; Ricci, D., Eds. Humana Press Inc, New Jersey, 2004, Vol. 242, pp 3-52.
87. Jain, P. K.; Huang, X.; El-Sayed, I. H.; and El-Sayed, M., *Acc. Chem. Res.* **2007**, *41*, 1578-1586.
88. Huang, W.; Qian, W.; El-Sayed, M. A., *Nano Lett.* **2004**, *4*, 1741-1747.
89. Kneipp, K.; Wang, Y.; Kneipp, H.; Perelman, L. T.; Itzkan, I.; Dasari, R. R.; Feld, M. S., *Phys. Rev. Lett.* **1997**, *78*, 1667-1670.
90. Nie, S.; Emory, S. R., *Science* **1997**, *275*, 1102-1106.
91. Campion, A.; Kambhampati, P., *Chem. Soc. Rev.* **1998**, *27*, 241-250.
92. Li, J. F.; Huang, Y. F.; Ding, Y.; Yang, Z. L.; Li, S. B.; Zhou, X. S.; Fan, F. R.; Zhang, W.; Zhou, Z. Y.; Wu, D. Y.; Ren, B.; Wang, Z. L.; Tian, Z. Q., *Nature* **2010**, *464*, 392-395.
93. Baker, G. A.; Moore, D. S., *Anal. Bioanal. Chem.* **2005**, *382*, 1751-1770.
94. Braun, G.; Lee, S. J.; Dante, T.; Nguyen, T. Q.; Moskovits, M.; Reich, N., *J. Am. Chem. Soc.* **2007**, *129*, 6378-6379.
95. Barhoumi, A.; Zhang, D.; Tam, F.; Halas, N. J., *J. Am. Chem. Soc.* **2008**, *130*, 5523-5529.
96. Guerrero, A. R.; Aroca, R. F., *J. Raman Spectrosc.* **2011**, DOI :10.1002/jrs.3065.
97. Oslon, L. G.; Lo, Y. S.; Beebe, T. P.; Harris, J. M., *Anal. Chem.* **2001**, *73*, 4268-4276.

98. Moore, B. D.; Stevenson, L.; Watt, A.; Flitsch, S.; Turner, N. J.; Cassidy, C.; Graham, D., *Nat. Biotechnol.* **2004**, *22*, 1133-1138.
99. Kneipp, J.; Kneipp, H.; Kneipp, K., *Chem. Soc. Rev.* **2008**, *37*, 1052-1060.
100. Sisco, P. N.; Murphy, C. J., *J. Phys. Chem. A* **2009**, *113*, 3973-3978.
101. Baik, S. Y.; Cho, Y. J.; Im, H. S.; Jang, D. M.; Myung, Y.; Park, J.; Kang, H. S., *ACS Nano*. **2012**, DOI:10.1021/nn204797b.
102. Ward, D. R.; Grady, N. K.; Levin, C. S.; Halas, N. J.; Wu, Y. P.; Nordlander, P.; Natelson, D., *Nano. Lett.* **2007**, *7*, 1396-1400.
103. Huang, W.; El-Sayed, I. H.; Qian, W.; El-Sayed, M. A., *Nano Lett.* **2007**, *7*, 1591-1597.
104. Sánchez-Iglesias, A.; Aldeanueva-Potel, P.; Ni, W.; Pérez-Juste, J.; Pastoriza-Santos, I.; Alvarez-Puebla, R. A.; Mbenkum, B. N.; Liz-Marzán, L. M., *Nano. Today* **2010**, *5*, 21-27.
105. Rycenga, M.; Wang, Z.; Gordon, E.; Copley, C. M.; Schwartz, A. G.; Lo, C. S.; Xia, Y., *Angew. Chem. Int. Ed.* **2009**, *48*, 9924-9927.
106. Lu, Y.; Lui, L.; Kim, J.; Mejia, X.; Lee, L. P., *Nano Lett.* **2005**, *5*, 119-124.
107. Gersten, J. I., *J. Chem. Phys.* **1980**, *72*, 5779-5780.
108. Schatz, G. C., *Acc. Chem. Res.* **1984**, *17*, 370-376.
109. Doering, W. E.; Piotti, M. E.; Natan, M. J.; Freeman, R. J., *Adv. Mater.* **2007**, *19*, 3100-3108.
110. Yang, M.; Chen, T.; Lau, W. S.; Wang, Y.; Tang, Q.; Yang, Y.; Chen, Y., *Small* **2009**, *5*, 198-202.
111. Su, X.; Zhang, J.; Sun, L.; Koo, W.-T.; Chan, S.; Sundararajan, N.; Yanmakawa, M.; Berlin, A. A., *Nano Lett.* **2005**, *5*, 49-54.

112. Orendorff, C. J.; Gole, A.; Sau, T.; C.J, M., *Anal. Chem.* **2005**, *77*, 3261-3266.
113. Stadler, J.; Schmid, T.; Zenobi, R., *Nanoscale* **2012**, *4*, 1856-1870.
114. Hayazawa, N.; Inouye, Y.; Sekkat, Z.; Kawata, S., *J. Chem. Phys.* **2002**, *117*, 1296-1301.
115. Hartschuh, A.; Sánchez, E. J.; Xie, X. S.; Novotny, L., *Phys. Rev. Lett.* **2003**, *90*, 095503-095507.
116. Deckert-Gaudig, T.; Deckert, V., *Phys. Chem. Chem. Phys.* **2010**, *12*, 12040-12049.
117. Lin, X.-D.; Uzayisenga, V.; Li, J.-F.; Fang, P.-P.; Wu, D.-Y.; Ren, B.; Tian, Z.-Q., *J. Raman Spectrosc.* **2012**, *43*, 40-45.
118. Amer, M. S. In *Raman Spectroscopy, Fullerenes and Nanotechnology*, Royal Society of Chemistry, Cambridge, 2010, pp 101-105.
119. Jung, H. Y.; Park, Y.-K.; Park, S.; Kim, S. K., *Anal. Chim. Acta* **2007**, *602*, 236-243.
120. Biggs, K. B.; Camden, J. P.; Anker, J. F.; Van Duyne, R. P., *J. Phys. Chem. A* **2008**, *113*, 4581-4586.
121. Galarreta, B. C.; Norton, P. R.; Lagugné-Labarhet, F., *J. Phys. Chem. C* **2010**, *114*, 19952-19957.
122. Natansohn, A.; Rochon, P., *Chem. Rev.* **2002**, *102*, 4139-4176.
123. Galarreta, B. C.; Rugar, I.; Young, A.; Lagugné-Labarhet, F., *J. Phys. Chem. C* **2011**, *115*, 15318-15323.
124. Jeanmaire, D. L.; Van Duyne, R. P., *J. Electroanal. Chem.* **1977**, *84*, 1-20.
125. Wang, X.; Qian, X.; Beitler, J. J.; Chen, Z. G.; Khuri, F. R.; Lewis, M. M.; Shin, H. J. C.; Nie, S.; Shin, D. M., *Cancer Res.* **2011**, *71*, 1526-1532.

126. Shang, L.; Brandholt, S.; Stockmar, F.; Trouillet, V.; Bruns, M.; Nienhaus, G. U., *Small* **2011**, DOI:10.1002/sml.201101353.
127. Tripathi, A.; Emmons, E. D.; Wilcox, P. G.; Guicheteau, J. A.; Emge, D. K.; Christensen, S. D.; Fountain, A. W., III, *Appl. Spectrosc.* **2011**, *65*, 611-619.
128. Osorio-Román, I. O.; Ortega-Vásquez, V.; Vargas C., V.; Aroca, R. F., *Appl. Spectrosc.* **2011**, *65*, 838-843.
129. Guieu, V.; Lagugné-Labarthe, F.; Servant, L.; Talaga, D.; Sojic, N., *Small* **2008**, *4*, 96-99.
130. Xu, J.; Zhang, L.; Gong, H.; Homola, J.; Yu, Q., *Small* **2011**, *7*, 371-376.
131. Moula, G.; Aroca, R. F., *Anal. Chem.* **2011**, *83*, 284-288.
132. Liz-Marzán, L. M.; Giersig, M.; Mulvaney, P., *Langmuir* **1996**, *12*, 4329-4335.
133. Moskovits, M., *Nature* **2010**, *464*, 357.
134. Guerrero, A. R.; Aroca, R. F., *Angew. Chem. Int. Ed.* **2011**, *50*, 665-668.
135. Aroca, R. F.; Teo, G. Y.; Mohan, H.; Guerrero, A. R.; Albella, P.; Moreno, F., *J. Phys. Chem. C* **2011**, *115*, 20419-20424.
136. Merlen, A.; Lagugné-Labarthe, F.; Harté, E., *J. Phys. Chem. C* **2010**, *114*, 12878-12884.
137. Bardhan, R.; Grady, N. K.; Halas, N. J., *Small* **2008**, *4*, 1716-1722.
138. Lu, G.; Li, W.; Zhang, T.; Yue, S.; Liu, J.; Hou, L.; Li, Z.; Gong, Q., *ACS Nano* **2012**, *6*, 1438-1448.
139. Kinkhabwala, A.; Yu, Z.; Fan, S.; Avlasevich, Y.; Müllen, K.; Moerner, W. E., *Nature* **2009**, *3*, 654-657.
140. Kelly, P. J.; Arnell, R. D., *Vacuum* **2000**, *56*, 159-172.

141. Thornton, J. A., *J. Vac. Sci. Technol. A* **1978**, *15*, 171-177.
142. Rossnagel, S. M.; Hopwood, J., *Appl. Phys. Lett.* **1993**, *63*, 3285-3287.
143. Yao, N.; Reyntjens, S.; Giannuzzi, L. A. In *Focused Ion Beam Systems*, Yao, N., Ed. Cambridge University Press, Cambridge, 2007, pp 1-9, 126-129.
144. Müller, M. In *Introduction to Confocal Fluorescence Microscopy*, 2nd ed.; International Society for Optical Engineering, Washington, DC, 2006, pp 1-21.
145. Gibson, K. F.; Correia-Ledo, D.; Couture, M.; Graham, D.; Masson, J.-F., *Chem. Commun.* **2011**, *47*, 3404-3406.
146. Yang, B.; Lu, N.; Qi, D.; Ma, R.; Wu, Q.; Hao, J.; Liu, X.; Mu, Y.; Reboud, V.; Kehagias, N.; Sotomayor Torres, C. M.; Boey, F. Y. C.; Chen, X.; Chi, L., *Small* **2010**, *6*, 1038-1043.
147. Mine, E.; Yamada, A.; Kobayashi, Y.; Konno, M.; Liz-Marzan, L. M., *J. Colloid Interface Sci.* **2003**, *264*, 385-390.
148. Desmedt, A.; Talaga, D.; Bruneel, J. L., *Appl. Spectrosc.* **2007**, *61*, 621-623.
149. Aslan, K.; Gryczynski, I.; Malicka, J.; Matveeva, E.; Lakowicz, J. R.; Geddes, C. D., *Curr. Opin. Biotechnol* **2005**, *16*, 55-62.
150. Cheng, D. M.; Xu, Q. H., *Chem. Commun.* **2007**, 248-250.
151. Zhang, J.; Matveeva, E.; Gryczynski, I.; Leonenko, Z.; Lackowicz, J. R., *J. Phys. Chem. B* **2005**, *109*, 7969-7975.
152. Lakowicz, J. R.; Shen, Y.; D'Auria, S.; Malicka, J.; Fang, J.; Gryczynski, Z.; Gryczynski, I., *Anal. Biochem.* **2002**, *301*, 261-277.
153. Pompa, P. P.; Martiradonna, L.; Della Torre, A.; Della Sala, F.; Manna, L.; De Vittorio, M.; Calabi, F.; Cingolani, R.; Rinaldi, R., *Nat. Nanotechnol.* **2006**, *1*, 126-130.



154. Szmecinski, H.; Lakowicz, J. R.; Catchmark, J. M.; Eid, K.; Anderson, J. P.; Middendorf, L., *Appl. Spectrosc.* **2008**, *62*, 733-738.
155. Chen, Y.; Munechika, K.; Ginger, D. S., *Nano Lett.* **2007**, *7*, 690-696.
156. Stranik, O.; Nooney, R.; McDonagh, C.; MacCraith, B., *Plasmonics* **2006**, *2*, 15-22.
157. Tovmachenko, O. G.; Graf, C.; van den Heuvel, D. J.; van Blaaderen, A.; Gerritsen, H. C., *Adv. Mater.* **2006**, *18*, 91-95.
158. Zhang, J.; Fu, Y.; Chowdhury, M. H.; Lakowicz, J. R., *J. Phys. Chem. C* **2008**, *112*, 9172-9180.
159. Gill, R.; Le Ru, E. C., *Phys. Chem. Chem. Phys.* **2011**, *13*, 16366-16372.
160. Leclair, A. M.; Ferguson, S. S. G.; Lagugné-Labarthe, F., *Biomaterials* **2010**, *32*, 1351-1360.

## Curriculum Vitae

**Name:** Shabila Fayyaz

**Post-secondary Education and Degrees:** Kinnaird College for Women  
Lahore, Pakistan  
2005-2009 B.Sc.Hons.

*The University of Western Ontario*  
London, Ontario, Canada  
2010-2012 M.Sc.

**Honours and Awards:** Western Graduate Research Scholarship (WGRS)  
2010-2011, 2011-2012

Western Graduate Scholarship  
2012

**Related Work Experience** Teaching Assistant  
*The University of Western Ontario*  
2010-2012

### Publications:

**Fayyaz, S.,** Tabatabaei, M-A., Lagurné-Labarthe F. (2012) Surface-Enhanced Fluorescence (SEF): Mapping Individual Hot-Spots in Silica-Protected 2D Gold Nanotriangle Arrays *Journal of Physical Chemistry C* . Submitted March, 2012.

### Posters:

Fayyaz, S. F. Lagurné-Labarthe (2011) “Cells Studies using SERS/ Fluoropolymer array.” 94<sup>th</sup> Canadian Chemistry Conference and Exhibition, Montreal, QC.

Fayyaz, S. F. Lagugné-Labarthe (2011) “Cells Studies using SERS/ Fluoropolymer array.” Centre for Advanced Materials and Biomaterials Research (CAMBR), London, ON.

Fayyaz, S. F. Lagugné-Labarthe (2011) “Cells Studies using SERS/ Fluoropolymer array.” ,NaNontario 2011, Hamilton, ON.